International Journal of Nanomedicine

ISSN: (Print) (Online) Journal homepage: www.tandfonline.com/journals/dijn20

Pretreatment of Human Umbilical Cord Mesenchymal Stem Cell-Derived Exosomes with Quercetin Enhances the Healing of Diabetic Skin Wounds by Modulating Host-Microbiota Interactions

Shuhui Wu, Zhongsheng Zhou, Yang Li, Ronghui Wu & Jinlan Jiang

To cite this article: Shuhui Wu, Zhongsheng Zhou, Yang Li, Ronghui Wu & Jinlan Jiang (2024) Pretreatment of Human Umbilical Cord Mesenchymal Stem Cell-Derived Exosomes with Quercetin Enhances the Healing of Diabetic Skin Wounds by Modulating Host-Microbiota Interactions, International Journal of Nanomedicine, , 12557-12581, DOI: 10.2147/IJN.S491471

To link to this article: https://doi.org/10.2147/IJN.S491471

Published online: 26 Nov 2024.

International Journal of Nanomedicine Dovepress

Open Access Full Text Article ORIGINAL RESEARCH

Pretreatment of Human Umbilical Cord Mesenchymal Stem Cell-Derived Exosomes with Quercetin Enhances the Healing of Diabetic Skin Wounds by Modulating Host-Microbiota Interactions

Shuhui Wu[1],*, Zhongsheng Zhou[1],*, Yang Li[1], Ronghui Wu[2], Jinlan Jiang[1]

[1]Scientific Research Center, China-Japan Union Hospital of Jilin University, Changchun, People's Republic of China; [2]Department of Dermatology, China-Japan Union Hospital of Jilin University, Changchun, People's Republic of China

*These authors contributed equally to this work

Correspondence: Jinlan Jiang, Scientific Research Center, China-Japan Union Hospital of Jilin University, Changchun, Jilin, 130033, People's Republic of China, Email jiangjinlan@jlu.edu.cn

Background: Owing to the distinctive advantages of mesenchymal stem cell-derived exosomes (MSCs-exo), these vesicles have emerged as a pivotal research focus in regenerative medicine, surpassing their MSC counterparts. Quercetin (Qr), widely recognized for its potent anti-inflammatory and antioxidant activities, demonstrates substantial potential in enhancing tissue repair processes. This study delves into the role of quercetin-pretreated MSC-derived exosomes ($MSCs^{Qr}$-exo) in accelerating the healing of diabetic wounds.

Methods: $MSCs^{Qr}$-exo were isolated from quercetin-pretreated MSCs and applied to fibroblasts to evaluate changes in cell function. An in vitro DSW rat model was also developed, and the rats were treated with $MSCs^{Qr}$-exo to assess wound healing progression. Fecal samples were collected for 16S rRNA sequencing and untargeted metabolomics to analyze changes in gut microbiota and metabolic profiles.

Results: $MSCs^{Qr}$-exo significantly enhanced fibroblast proliferation and migration while improving the therapeutic efficacy of MSCs-exo in DSW treatment. Gut microbiota and metabolomic analyses revealed marked changes in DSW rats, with $MSCs^{Qr}$-exo effectively alleviating dysbiosis. $MSCs^{Qr}$-exo upregulated Faecalibacterium abundance and regulated arachidonic acid metabolism in both the arachidonic and linoleic acid pathways. Firmicutes and Enterobacteriaceae influenced the arachidonic acid pathway by modulating 14.15-EET expression levels.

Conclusion: $MSCs^{Qr}$-exo facilitate DSW wound healing through modulation of dysbiotic gut microbiota linked to DSW pathology. This discovery offers novel therapeutic avenues and research trajectories for enhancing DSW recovery.

Keywords: mesenchymal stem cells, exosomes, quercetin, diabetic skin wound, gut microbiota, metabolites

Introduction

As a widely acknowledged global public health concern, diabetes has been confirmed to be a metabolic disorder shaped by interactions among immune, genetic, psychological, environmental, and other factors.[1] With the worsening issue of global aging, the incidence of diabetes is showing a year-on-year rise worldwide.[2] In recent years, the onset age of diabetes has been progressively declining, and due to its chronic course and numerous complications, diabetes profoundly affects both the health status and economic expenditures of patients. As the disease advances, sustained hyperglycemia disrupts not only the homeostasis of the internal environment but also induces chronic damage and dysfunction in various tissues of the body. Ultimately, this results in irreversible damage to organs and tissues, leading to a range of complications. Diabetic skin wounds(DSW) are particularly prevalent among these complications. Inadequate control post-onset can lead to limb necrosis, significantly elevating disability rates.[3] This disease is marked by its chronicity, complexity, and poor prognosis, profoundly impacting patients' quality of life and imposing considerable economic burdens on both individuals and society.[4] Current conventional clinical treatment

Received: 9 September 2024
Accepted: 20 November 2024
Published: 26 November 2024

Graphical Abstract

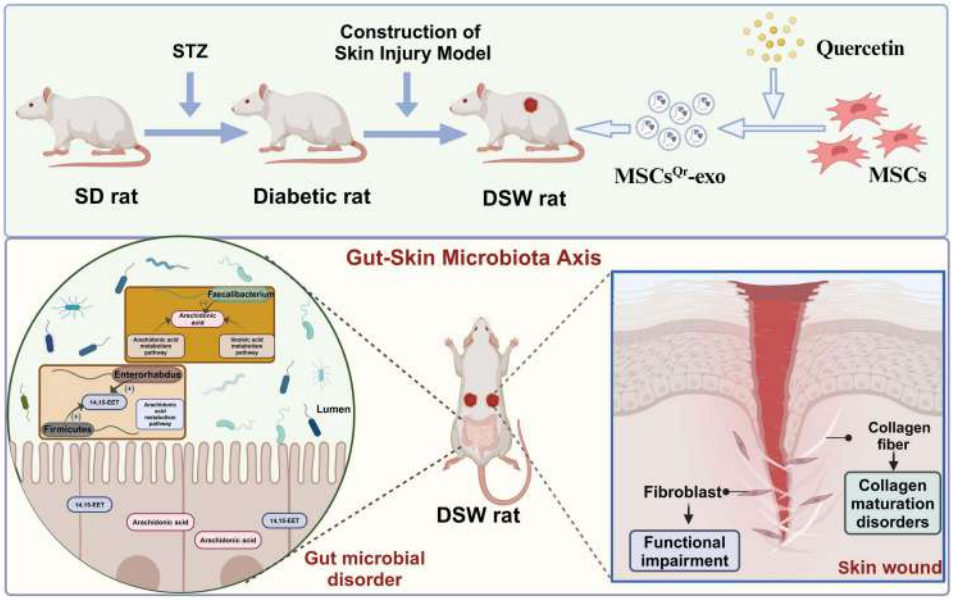

methods encompass blood glucose control, wound dressing changes, hyperbaric oxygen therapy, negative pressure wound therapy, total contact casting, wound debridement, tissue grafting, among others.[5] Nevertheless, these therapeutic approaches are fraught with limitations; they merely alleviate symptoms or postpone disease advancement without rectifying impaired blood vessels and nerves. Furthermore, wounds continue to present challenges in healing.

Mesenchymal stem cells (MSCs) are cells known for their pronounced paracrine functions, immunoregulatory capabilities, homing properties, and multipotent differentiation potential. Current research has solidified MSCs' profound therapeutic impact on inflammation-related disorders.[6] Recent investigations have further underscored MSCs' pivotal roles in fostering vascular regeneration, mitigating inflammatory reactions, contributing to extracellular matrix remodeling, and facilitating wound healing.[7–10] Exosomes are extracellular vesicles secreted by MSCs, ranging in diameter from 30 to 150 nm, facilitating intercellular communication through the transfer of signaling molecules like non-coding RNAs and proteins.[11] Exosomes serve as exceptional mediators of intercellular communication due to several unparalleled advantages: their nanoscale size facilitates unrestricted intercellular transfer, their unique phospholipid bilayer structure safeguards bioactive substances from degradation during transit, and their surface is enriched with specific proteins that enhance targeting capabilities.[12] Additionally, as a cell-free therapy, exosomes offer advantages over MSCs such as superior stability, reduced immunogenicity, and no risk of tumorigenesis.[13] Studies have demonstrated that exosomes secreted by MSCs (MSCs-exo) exhibit therapeutic effects similar to those of MSCs.[14] Hence, the presence of MSCs-exo makes cell-free therapies for wound healing feasible.[15]

According to previous studies on diabetic skin wounds, diabetic patients face challenges in wound healing due to a combination of factors such as hyperglycemic stimulation, abnormal wound microenvironment, microvascular obstruction, impaired angiogenesis, and altered macrophage phenotypes.[16] The pathogenesis of DSW is complex and not fully elucidated. Recently, the indispensable role of gut microbiota in maintaining host physiological health has garnered widespread attention.[17] The gut microbiota constitutes a complex ecological community that plays a crucial role within the host.[18] Research indicates that lipopolysaccharides (LPS) from gut microbiota bacteria promote chronic subclinical inflammation and induce insulin resistance through TLR4 activation.[19] Importantly, microbial communities also play a significant role in the healing and clinical outcomes of chronic diabetic foot ulcers.[20] Hence, it can be inferred that gut microbiota may also play a significant role in diabetic skin wound healing. Recent studies have widely demonstrated the

significant role of MSCs-exo in the modulation of gut microbiota. Research indicates that MSCs-exo can effectively restore OTU structural changes and counteract α-diversity reduction induced by colitis, through modulation of the gut metagenome-metabolome-fxr axis. This process not only increases beneficial microbial abundance but also reduces pathogenic bacteria, suppresses detrimental functions, and simultaneously enhances other critical cellular functions, thereby optimizing gut microbiota composition. These findings reveal potential therapeutic targets for colitis treatment.[21] Exosomal miR-150-3p derived from MSCs mediates therapeutic effects by modulating the abundance of key microbial groups, including Proteobacteria, Muribaculaceae, Lachnospiraceae_NK4A136_group, and Acinetobacter, in the gut microbiota of intracerebral hemorrhage (ICH) model mice.[22] MSCs-exo modulate serum metabolites and gut microbiota in liver trauma models, thereby facilitating tissue repair. This discovery offers novel insights into the anti-inflammatory potential of MSCs-exo in liver trauma models.[23] Collectively, these findings suggest that MSCs-exo may play a crucial role in countering disease-induced gut microbiota dysbiosis, prompting further investigation into whether exosomes may enhance recovery by modulating gut microbiota in DSW rat models.

In recent years, multiple studies have shown that pre-treating MSCs with drugs, cytokines, physical factors, and other methods enhances their bioactivity and functionality in tissue regeneration.[24,25] Pretreated MSCs exhibit significantly enhanced paracrine effects. It has been reported that diabetic wounds contain high levels of neutrophil extracellular traps (NETs), which activate endoplasmic reticulum stress and impair fibroblast function, thereby playing a crucial role in delaying diabetic wound healing. MSCs-exo pretreated under hypoxia can improve diabetic wound healing by influencing miR-17-5p and inhibiting excessive NETs formation.[26] Compared to normal MSCs-exo, exosomes secreted by MSCs pretreated with pioglitazone (PGZ-Exos) exhibit a more pronounced effect in promoting angiogenesis, offering greater advantages in promoting diabetic wound healing.[27] Melatonin-stimulated MSCs secrete exosomes that modulate macrophage polarization via the PTEN/AKT pathway, exerting a more significant role in promoting diabetic wound healing.[28] Quercetin (Qr) is a natural flavonoid compound known for its potent antioxidant and anti-inflammatory properties.[29] Widely found in the stems and leaves of fruits and vegetables consumed daily, quercetin has been established to possess significant medicinal value. Research has demonstrated its beneficial effects in inflammatory diseases.[30] Moreover, quercetin has been shown to stimulate angiogenesis and promote fibroblast proliferation.[31] Given these characteristics, quercetin plays a crucial role in improving diabetic wound healing processes. Unfortunately, the impact of quercetin on MSCs-exo and its role in diabetic skin wound healing have not been studied. Pretreating MSCs with quercetin and isolating their secreted exosomes ($MSCs^{Qr}$-exo), we aim to compare the effects of MSCs-exo and $MSCs^{Qr}$-exo in promoting diabetic wound healing.

In conclusion, studying the interaction between gut microbiota and DSW may serve as a novel therapeutic strategy for DSW. Therefore, we hypothesize that $MSCs^{Qr}$-exo, compared to MSCs-exo, may exert a more pronounced effect on gut microbiota and metabolite modulation, thereby enhancing DSW healing more efficiently. To test this hypothesis, fibroblasts will be exposed to high glucose concentrations to simulate diabetic in vitro conditions at the cellular level. Fibroblasts will then be treated with MSCs-exo or $MSCs^{Qr}$-exo, and their proliferation and migration capabilities will be observed. Simultaneously, a DSW rat model will be established to compare the wound healing efficacy of MSCs-exo and $MSCs^{Qr}$-exo. Fecal samples will be collected from the rats for 16S rRNA amplicon sequencing and untargeted metabolomics analysis.

Methods and Materials

Preparation and Characterization of MSCs

The umbilical cord tissue was isolated and collected, followed by three washes with phosphate-buffered saline (PBS, Sigma, Germany), and then cut into tissue fragments. The isolated tissue fragments were placed in 100 mm culture dishes (Corning, USA), with 10 mL of culture medium added to each dish. The culture medium used was DMEM (Stem cell, Canada) supplemented with 20% fetal bovine serum (Corning, USA). The distance between each tissue fragment was approximately 3 millimeters. The cultures were maintained in a 37°C humidified CO_2 incubator (Thermo Fisher, USA). The culture medium in the dishes was changed every three days, and cell growth was monitored. When the cell density

around the tissue reached 80%, cells were passaged using α-MEM medium supplemented with 10% fetal bovine serum and 1% penicillin/streptomycin (HyClone, USA). Cells used in the experiments were from passages 3 to 6 of MSCs.

MSCs were cultured in adipogenic differentiation medium (Sigma, Germany) for approximately 18–21 days. Oil Red O staining solution (Solarbio, China) was applied for 10–20 minutes after cultivation, followed by microscopic observation and photography. For osteogenic differentiation of MSCs, osteogenic differentiation medium (Sigma, Germany) was used, and after approximately 28 days, cells were stained with Alizarin Red (Solarbio, China) for 20–30 minutes. The cells were then observed under a microscope and documented. MSCs underwent chondrogenic differentiation using chondrogenic differentiation medium (Sigma, Germany) for approximately 21 days, forming cartilage pellets. Sections were stained with Alcian Blue (Solarbio, China) for about 30 minutes, washed multiple times with water, followed by brief staining with Nuclear Fast Red for approximately 5 minutes, and then photographed under a microscope. MSCs were characterized using flow cytometry with a panel of antibodies: PE-conjugated anti-human CD45, FITC-conjugated anti-human CD90 (Thy1), PE-conjugated anti-human CD73 (Ecto-5'-nucleotidase), FITC-conjugated anti-human CD11b, FITC-conjugated anti-human CD19, FITC-conjugated anti-human CD34, PE-conjugated anti-human CD105, and PE-conjugated anti-human HLA-D, all sourced from Biolegend, USA.

Isolation and Characterization of MSCs-Exo and MSCs^{Qr}-Exo

Human umbilical cord-derived MSCs were collected and cultured, and conditioned medium from passages 3 to 6 MSCs was collected during culture. Initially, the conditioned medium was centrifuged at 200 g for 10 minutes to remove dead cells. Subsequently, centrifugation at 2000 g for 10 minutes was performed to eliminate cellular debris, followed by centrifugation at 10,000 g for 1 hour to remove microvesicles. Finally, MSCs-exo were isolated through centrifugation at 100,000g for 1 hour.

Quercetin (HPLC≥98%) was purchased from Yuanye Biotechnology Co., Ltd. (Shanghai, China). To isolate MSCs^{Qr}-exo, quercetin was added to α-MEM culture medium supplemented with 10% fetal bovine serum and 1% penicillin/streptomycin to pretreat the MSCs; after 48 hours, the medium was collected. MSCs^{Qr}-exo were then isolated using the aforementioned ultracentrifugation method.

The morphology of MSCs-exo and MSCs^{Qr}-exo was observed using an 80 kV transmission electron microscope (TEM; Hitachi, Japan). Nanoparticle tracking analysis (NTA, NanoSight LM10, UK) was utilized to determine the size and concentration of MSCs-exo and MSCs^{Qr}-exo.

Western Blot

Western blot analysis was conducted to detect Calnexin, TSG101, CD63, type I collagen, and type III collagen. After treating cells or tissues with radioimmunoprecipitation assay (RIPA) buffer (Abcam, USA) containing 1 mmol/L phenylmethylsulfonyl fluoride (PMSF, Thermo Fisher Scientific), MSCs-exo and MSCs^{Qr}-exo were centrifuged at 16,000g for 15 minutes to collect their protein samples. Protein concentration was determined using a BCA assay kit (Beyotime, China), followed by denaturation at 95°C for 5 minutes. Following separation by SDS-PAGE gel electrophoresis, proteins were transferred onto Nitrocellulose (NC) membranes (Millipore, Germany). After blocking with 5% skim milk powder for 1 hour, NC membranes were incubated overnight at 4°C with primary antibodies against CD63 (1:1000, Proteintech, China), TSG101 (1:4000, Proteintech, China), Calnexin (1:10000, Proteintech, China), type I collagen (1:10000, Proteintech, China), type III collagen (1:10000, Proteintech, China) and β-actin (1:50000, Proteintech, China). The next day, after washing the NC membranes three times with TBST, proteins were detected by incubating with corresponding secondary antibodies (1:5000, Proteintech, China) at room temperature for 1 hour.

Cell Proliferation Assay

The CCK-8 assay was employed to evaluate changes in HSF proliferation in response to MSCs-exo and MSCs^{Qr}-exo treatments. HSF cells were uniformly seeded into a 96-well plate. Culture media containing graded concentrations of MSCs-exo or MSCs^{Qr}-exo (0, 5, 10, and 20 μg/mL) were prepared, followed by co-culture with HSFs. Absorbance at 450 nm was measured using a microplate reader (Synergy H1; BioTek).

Labeling and Uptake Experiments of Exosomes

MSCs-exo and MSCs^{Qr}-exo were incubated with Dio dye (Sigma, USA) for 30 minutes, and subsequently subjected to high-speed centrifugation to remove excess dye. Labeled MSCs-exo and MSCs^{Qr}-exo were incubated with human skin fibroblasts (HSF) for 24 hours. After fixation with 4% paraformaldehyde, cells were stained with 4′,6-diamidino-2-phenylindole (DAPI; Solarbio, China) for 5 minutes to visualize HSF nuclei. Laser confocal scanning microscopy (CLSM) (Olympus FV1000, Japan) was employed to observe exosome uptake and capture images.

EdU Incorporation Assay

The proliferation capability of HSF was assessed using the 5-ethynyl-2'-deoxyuridine (EdU) incorporation assay (Servicebio, China). Fibroblasts were seeded into 96-well plates, and after cell adhesion, 10 μM EdU reagent was added to each well, followed by incubation at 37°C for 2 hours. Staining procedures were carried out according to the manufacturer's instructions. Stained results were visualized and recorded using a fluorescence microscope (Olympus, Japan). EdU labeling rate (%) = Number of EdU-positive cells / (Number of EdU-positive cells + Number of EdU-negative cells)×100%.

Transwell Assay

Using Transwell chambers equipped with polycarbonate membranes (Corning, Corning, NY, USA) that have 8 mm pores, we assessed the migration capability of HSF. Each upper chamber was seeded with an equal number of cells suspended in 0.2 mL of DMEM medium lacking FBS (HyClone, USA), which were prepared from HSF cells resuspended following different treatments. The lower chamber was filled with complete growth medium. The chambers were then placed in a 37°C, 5% CO2 atmosphere for 24 hours. The next day, cells were fixed with 4% paraformaldehyde for 15 minutes, washed three times with PBS, and stained with 0.1% crystal violet for 10 minutes. After gently removing surface cells with a cotton swab, cell migration was observed and documented under an Olympus optical microscope.

Animal Model

Male specific pathogen-free (SPF) SD rats, aged 7–8 weeks and weighing 200–220g, were procured from Beijing Huafukang Biotechnology Co., Ltd. They were housed at the School of Public Health, Jilin University (SYXK(JI)2021–0003), where they were maintained under standard conditions including 50%-60% relative humidity, a 12-hour light/dark cycle, free access to food and water, and an ambient temperature of approximately 25°C. This study was conducted under the supervision of the Institutional Animal Care and Use Committee (IACUC) at the School of Public Health, Jilin University, in strict accordance with GB2018-35,892 - Guidelines for Ethical Review of Laboratory Animal Welfare, with all housing conditions stringently following the standards of GB14925. The study was approved under the title "Mechanistic Investigation of MSCs^{Qr}-exo in Promoting Wound Healing in Diabetic Skin Injury in Rats" with approval number 202411001. The experimental procedures strictly adhered to the ethical guidelines of Jilin University and national regulations governing the welfare of laboratory animals. This study was conducted in accordance with the principles outlined in the Helsinki Declaration.

Following a 3-day acclimatization period, rats were randomly divided into a control group (n=8) and a model group (n=40). Rats in the model group underwent overnight fasting and water deprivation. The following day, they received an intraperitoneal injection of STZ (55 mg/kg, Sigma, USA) dissolved in a citrate buffer solution at pH 4.5, with injections prepared within 15 minutes. To mitigate early mortality caused by partial pancreatic islet damage and subsequent insulin release, rats were provided with drinking water containing 15g/L sucrose after STZ injection. The following day after injection, blood glucose levels of each group of rats were measured using a glucometer, with subsequent measurements taken every other day. Diabetes was defined if blood glucose levels exceeded 16.7 mmol/L in four consecutive measurements.

Each group of rats was anesthetized by intraperitoneal injection of 1% pentobarbital sodium (40 mg/kg), positioning them in a prone position after induction. The dorsal fur was removed, and a full-thickness incision with a diameter of 1.8 cm was made on the back of each rat. A total of 32 successfully modeled rats from the model group were randomly

selected and divided into four groups (n=8): the model group received an injection of 200 μL PBS, the Quercetin group received 5 mg/kg Quercetin, and the MSCs-exo and MSCs^{Qr}-exo groups each received injections of 500 μg/kg exosomes. Treatment was administered using a combination of multi-site subcutaneous injections and tail vein injections. Following injections, each rat's wounds were covered with occlusive dressings (Tegaderm™; 3M™, USA). Photographs of the surgical wounds of the rats were taken on days 0, 7, 14, and 21 post-operation. A detailed timeline of the in vivo study is illustrated in Figure 1.

Histological Analysis

On day 21, tissue samples from the rat wound sites were collected and fixed in 4% paraformaldehyde. After dehydration, the wound tissues were embedded in paraffin. Sections approximately 5μm thick were prepared and subjected to Hematoxylin & eosin (HE) staining and Masson's trichrome staining to observe wound length and collagen maturity.

Immunohistochemistry Staining Analysis

After deparaffinization and hydration of the sections, they were incubated overnight at 4°C with primary antibodies against collagen I, collagen III, α-SMA, ki67, and TGFβ-1 (diluted 1:100, Proteintech, China). The next day, the sections were incubated at room temperature for 30 minutes with corresponding secondary antibodies (diluted 1:2000, Proteintech, China). Finally, DAB chromogen was used for visualization, followed by counterstaining with hematoxylin.

16S ribosomal ribonucleic acid (16S rRNA) amplicon sequencing

The 16S rRNA amplicons were sequenced by Gensky Biotechnology Co., Ltd., located in Shanghai, 201315 (China). Total genomic DNA extraction was performed using the FastDNA® SPIN Kit for Soil (MP Biomedicals, Santa Ana, CA). The integrity of the extracted DNA was assessed via agarose gel electrophoresis, and its purity and concentration were determined using Nanodrop 2000 and Qubit 3.0 spectrophotometers. The V3V4 hypervariable region of the 16S rRNA gene was amplified using specific primers, followed by sequencing on the Illumina NovaSeq 6000 desktop sequencer.

Metabolomics Analysis

After weighing the samples, an appropriate amount was transferred into 2 mL EP tubes. Next, 600 μL of methanol solution containing 4 ppm 2-chloro-L-phenylalanine (stored at −20°C) was added, followed by vortexing for 30s with steel beads in a tissue grinder at 50 hz for 120 s. Ultrasonication was performed for 10 min at room temperature. Subsequently, the mixture was centrifuged at 12,000 rpm for 10 min at 4°C, and the supernatant was filtered through a 0.22 μm membrane filter into a detection vial. From each sample to be tested, 20 μL was taken to prepare QC samples (QC refers to correcting deviations in the analysis results of the mixed samples and errors caused by machine reasons; QC injection testing is usually performed when the number of experimental samples > 10, and may be omitted when the number of samples ≤ 10); the remaining samples were subjected to LC-MS analysis.

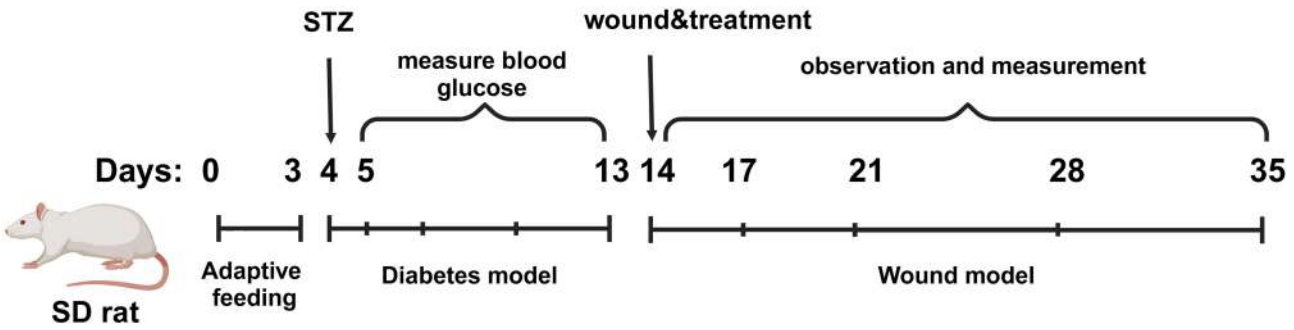

Figure 1 Schematic timeline of the animal model establishment.

Statistical analyses

Data analysis was performed using GraphPad Prism 9.0 (GraphPad Software Inc; La Jolla, CA, USA). Each experimental dataset is presented as the mean ± SD of no fewer than three independent experiments. Differences between the two groups were compared using a *t*-test. Multiple comparisons among more than two groups were conducted using Tukey's post hoc test following one- or two-way ANOVA to analyze differences. A difference was considered statistically significant when $P < 0.05$.

Results

Characterization of MSCs and Exosomes

As the trilineage differentiation results of MSCs can reflect their differentiation potential, we assessed the trilineage differentiation potential of MSCs and simultaneously examined MSC surface markers. Following osteogenic differentiation, distinct red calcium nodules were observed within the cells (Figure 2A). Adipogenic differentiation of MSCs revealed the presence of lipid droplets within the cells (Figure 2B). Cartilage spheroid sections stained with Alcian blue exhibited a blue coloration (Figure 2C). Surface markers of MSCs were characterized using flow cytometry. The results indicated that MSCs were positive for CD90, CD105, and CD73, but negative for CD11b, CD19, CD34, CD45, and HLA-DR (Figure 2D).

To investigate the role of $MSCs^{Qr}$-exo in the healing process of DSW, exosomes were isolated from the supernatants of MSCs and quercetin-pretreated MSCs ($MSCs^{Qr}$) using gradient ultracentrifugation. Transmission electron microscopy revealed that both MSCs-exo and $MSCs^{Qr}$-exo exhibited the typical bilayer membrane structure (Figure 2E). Western blot analysis was employed to detect exosomal surface markers, revealing that both MSCs-exo and $MSCs^{Qr}$-exo expressed typical exosomal markers such as TSG101 and CD63, with minimal expression of Calnexin. Protein expression levels showed no significant differences (Figure 2F). Nanoparticle tracking analysis (NTA) was used to measure the particle size distribution of MSCs-exo and $MSCs^{Qr}$-exo, demonstrating that the majority of MSCs-exo and $MSCs^{Qr}$-exo particles were distributed in the 100–150 nm range (Figure 2G–H). The results of various assays indicate that MSCs-exo and $MSCs^{Qr}$-exo share similar morphology, particle size distribution, and protein expression profiles. Quercetin pretreating of MSCs did not alter the characteristics of the exosomes they secrete.

$MSCs^{Qr}$-Exo Enhances the Proliferation and Migration Capabilities of HSFs Under High-Glucose Conditions

Fibroblasts play a crucial role in the wound healing process. Therefore, we utilized HSFs in vitro to validate the role of $MSCs^{Qr}$-exo in wound healing. Initially, we labeled MSCs-exo and $MSCs^{Qr}$-exo with Dio and co-incubated them with HSFs. Both MSCs-exo and $MSCs^{Qr}$-exo were internalized by HSFs, and there was no statistically significant difference in their uptake levels (Figure 3A–B). Different doses of MSCs-exo and $MSCs^{Qr}$-exo were applied to HSF cells, followed by CCK-8 assays. The results indicated that HSF cells treated with MSCs-exo and $MSCs^{Qr}$-exo exhibited enhanced proliferation to varying degrees, with this enhancement showing a dose-dependent effect (Figure S1 A-B). A concentration of 10 μg/mL of MSCs-exo and $MSCs^{Qr}$-exo was selected to treat HSF cells in order to further examine their effects on HSF proliferation and migration. In order to evaluate the effects of $MSCs^{Qr}$-exo on HSF function, PBS, quercetin, MSCs-exo, and $MSCs^{Qr}$-exo were individually administered to HSF cells induced by high glucose (HG) to monitor alterations in their proliferation and migration abilities. The EDU incorporation method was employed to evaluate the proliferation levels of HSF cells. In comparison to the non-high glucose-induced control group, the proliferation capacity of HSF cells in the model group was notably diminished. Conversely, in the HG-induced HSF group, all treatment groups demonstrated varying degrees of enhancement. Notably, the $MSCs^{Qr}$-exo treatment exhibited the most pronounced enhancement in the proliferation capacity of HG-induced HSF cells (Figure 3C–D). The migration ability of HSF cells was evaluated using the Transwell assay following various treatments. Following high glucose induction, HSF cell migration was markedly reduced compared to the control group. Subsequent treatments with quercetin, MSCs-exo, and $MSCs^{Qr}$-exo showed varying degrees of enhancement in migration ability. Notably, the $MSCs^{Qr}$-exo treatment demonstrated the most substantial improvement (Figure 3E–F).

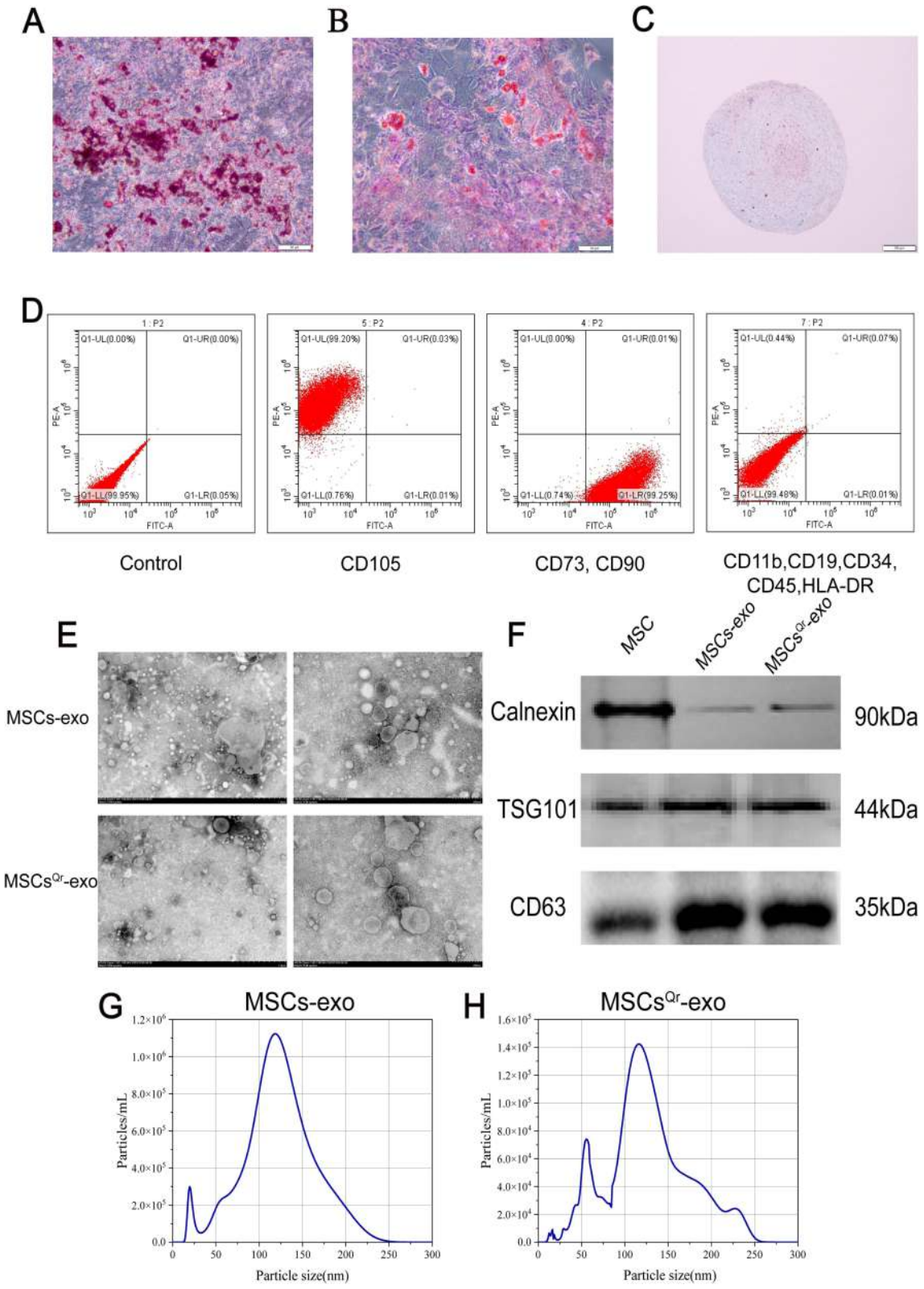

Figure 2 Characterization of MSCs and their derived exosomes. (**A**) Representative images of osteogenic differentiation of MSCs. Scale bar=50μm. (**B**) Representative images of adipogenic differentiation of MSCs. Scale bar=50μm. (**C**) Representative images of chondrogenic differentiation of MSCs. Scale bar = 100 μm. (**D**) Identification of MSC surface markers by flow cytometry. (**E**) Representative TEM images of MSCs-exo and MSCs^{Qr}-exo. Left: scale bar = 1 μm, Right: scale bar = 200 nm. (**F**) Characterization of MSCs-exo and MSCs^{Qr}-exo by Western blot analysis. (**G** and **H**) Characterization of MSCs-exo and MSCs^{Qr}-exo by nanoparticle tracking analysis.

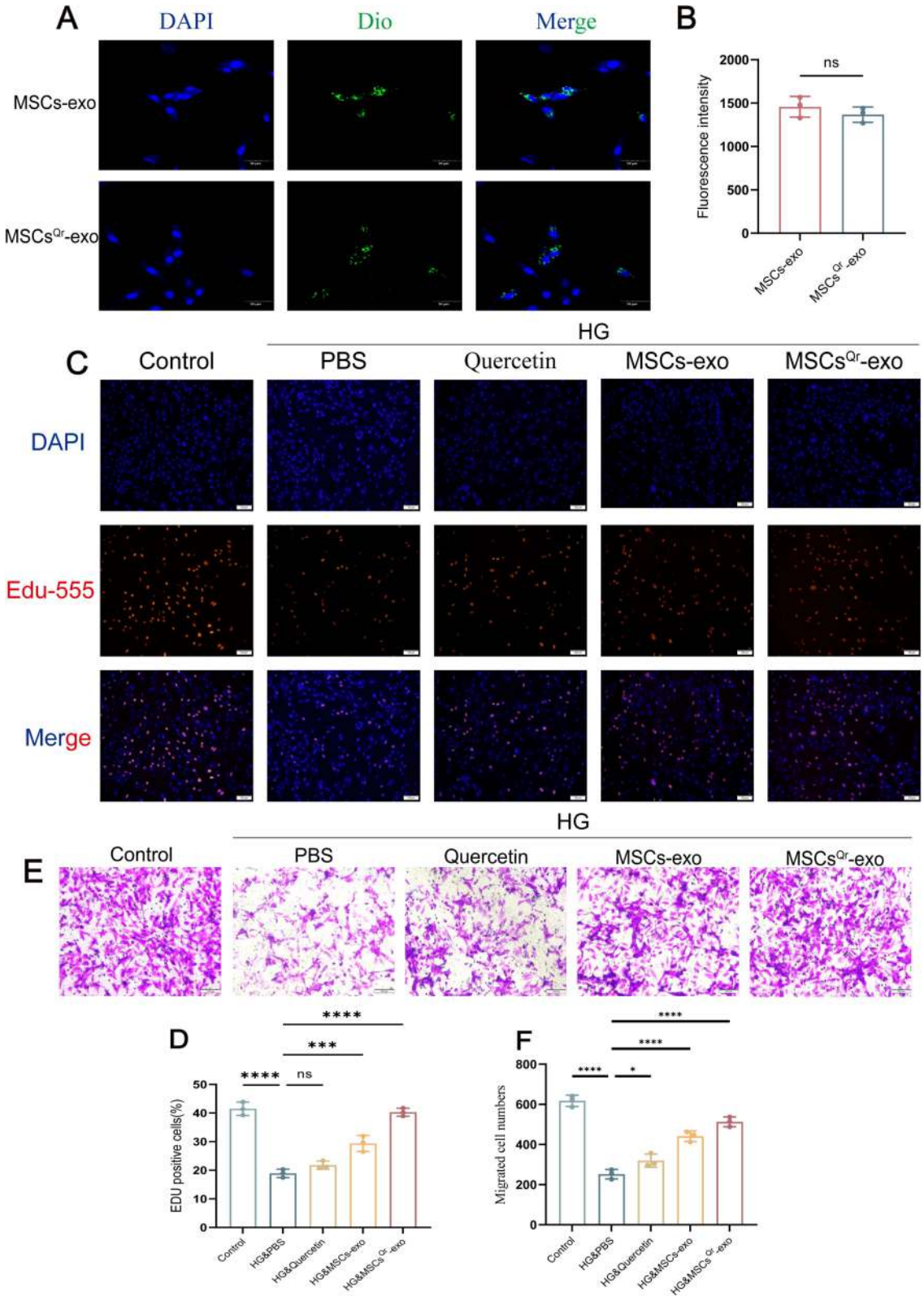

Figure 3 MSCs^{Qr}-exo enhances the proliferation and migration capabilities of HSFs induced by HG. (**A** and **B**) Uptake of Dio-labeled MSCs-exo and MSCs^{Qr}-exo by HSFs observed via laser scanning confocal microscopy. Nuclei and exosomes are stained blue and green, respectively. Scale bar = 50 μm. Statistical significance: ns: no significance. The figure employs double-headed error bars to represent the 95% confidence interval of the data. (**C** and **D**) Proliferation of high glucose-induced HSFs treated with quercetin, MSCs-exo, MSCs^{Qr}-exo, or untreated, assessed by Edu assay. DAPI: blue; Edu555: red. Scale bar = 100 μm. (**E** and **F**) Migration abilities of fibroblasts treated with different methods assessed by Transwell assay; scale bar = 200 μm. Compared with the HG&PBS group: ns: no significance, *p < 0.05, ***p < 0.001, ****p < 0.0001. The figure employs double-headed error bars to represent the 95% confidence interval of the data.

MSCs^{Qr}-Exo Enhances Wound Healing in Skin Wounds of Diabetic Rats Induced by STZ

To further validate the therapeutic efficacy of MSCs^{Qr}-exo in diabetic skin wound healing, SD rats were induced with diabetes by STZ injection. Blood glucose levels were monitored on days 1, 3, 5, 7, and 9 post-injection to confirm successful model establishment (Figure 4A). Considering the classic symptoms of diabetes ("polyuria, polydipsia, polyphagia, and weight loss"), observations were made on diet, water intake, and bedding moisture levels across groups, while also documenting changes in body weight (Figure 4B). In comparison to the control group, all STZ-induced diabetic rats exhibited markedly elevated blood glucose levels and significant weight loss. Furthermore, rats with successfully induced models displayed typical symptoms of increased diet, water intake, and urine output, validating the establishment of the diabetic rat model. Following this confirmation, a full-thickness skin defect model was created on the dorsal skin of these rats to evaluate wound healing outcomes after various treatments. Macroscopic evaluations of wound closure were performed on days 0, 7, 14, and 21 (Figure 4C–F). In comparison to the control group, the model group demonstrated a markedly slower wound healing rate, which was ameliorated by different treatment modalities across all groups. Among these, the MSCs^{Qr}-exo group showed the most favorable therapeutic efficacy, significantly promoting the healing of diabetic skin wounds. HE staining was employed to evaluate the wound length in each group. The findings indicated that, compared to both the quercetin and MSCs-exo groups, the MSCs^{Qr}-exo group exerted a more pronounced effect in enhancing the healing of skin injuries in diabetic rats (Figure 5A–B). Masson's trichrome staining results showed that collagen expression in the local wound area of the model group was relatively sparse. After treatment with MSCs^{Qr}-exo, it demonstrated a more compact collagen synthesis capability, suggesting MSCs^{Qr}-exo's superior role in promoting extracellular matrix (ECM) remodeling (Figure 5C–D). Immunohistochemical staining results indicated that MSCs^{Qr}-exo showed significant advantages in enhancing the synthesis of type I collagen and type III collagen (Figure 5E–G). Western blot results provided additional validation for this conclusion (Figure 5H, Figure S2A-B). Furthermore, assessment of molecular markers associated with wound healing, including α-SMA, Ki67, and TGF-β1, via immunohistochemical staining, consistently confirmed that MSCs^{Qr}-exo demonstrated better therapeutic effects in promoting diabetic skin wound healing (Figure 6A–D). These findings collectively validate the significant role of MSCs^{Qr}-exo in enhancing diabetic skin wound healing.

Integration of Multi-Omics Confirms That Microbial-Host Interactions Represent a Potential Novel Mechanism in DSW Rats

To investigate the changes in gut microbiota following DSW occurrence, we conducted an extensive analysis of gut microbial communities in DSW rats and control groups. Fecal samples were collected from DSW rats and subjected to 16S rRNA sequencing. Analysis of gut-specific OTUs in control and model group rats revealed 2464 OTUs in the model group and 1785 OTUs in the control group, with 875 OTUs shared between both groups (Figure 7A). Cluster analysis revealed significant differences in fecal composition between the model and control groups of rats (Figure 7B). Principal Coordinate Analysis (PCoA) based on unifrac distances was employed for Beta diversity analysis.[32] Each point in the graph represents a sample, with colors indicating different sample groups. Points closer together indicate greater similarity between samples. The graph clearly indicates that there is no overlap between the model and control groups, demonstrating effective intergroup separation in variability. Additionally, intra-group differences are not significant, suggesting high similarity between samples. These results indicate that the gut microbiota of rats in the model group undergo changes compared to the control group (Figure 7C). The bar charts of samples provide a visual representation of each sample's functional composition, the consistency of species composition within each group, and the intergroup functional differences. Microbial composition at the phylum and genus levels was analyzed and compared, with species with relative abundances >1% selected for the bar charts. Experimental results demonstrate significant differences in the gut microbiota composition between the model and control groups of rats at both the phylum and genus levels. At the phylum level analysis, both the control and model groups were predominantly composed of Firmicutes, Bacteroidetes, and Proteobacteria. Compared to the control group, the model group exhibited significant changes in Firmicutes and Bacteroidetes. Specifically, Firmicutes were significantly reduced while Bacteroidetes showed a marked increase in the model group (Figure 7D). These findings were further validated by box plots generated from Metastats analysis (Figure 7E). At the genus level analysis, the model group showed a significant

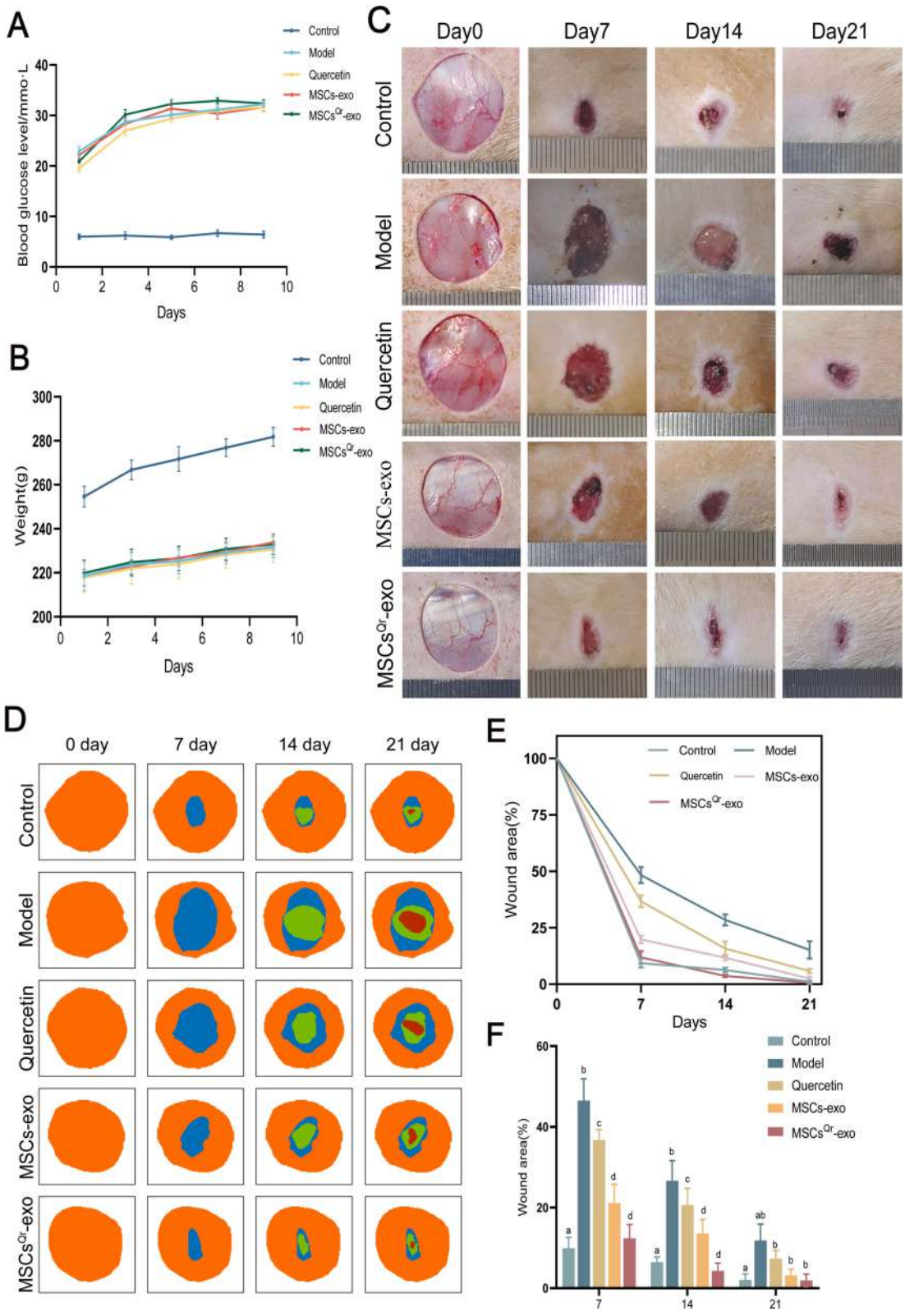

Figure 4 MSCs^{Qr}-exo significantly promotes wound healing in DSW. (**A**) Blood glucose levels were measured on days 1, 3, 5, 7, and 9 after STZ injection in each group of rats. (**B**) Body weight was measured on days 1, 3, 5, 7, and 9 after STZ injection in each group of rats. (**C**) Representative images of wounds were captured on days 0, 7, 14, and 21 after establishment of the DSW rat model. (**D**) Image simulation of wound closure area was conducted using ImageJ software. (**E**) Quantitative assessment of wound closure rates was performed for each group. (**F**) Wound closure rates were compared at different treatment times. N = 6. Data were analyzed using Tukey's multiple comparisons test, with "a, b, c, d" in the figure indicating significant differences between groups at a significance level of $p < 0.05$. The figure employs double-headed error bars to represent the 95% confidence interval of the data.

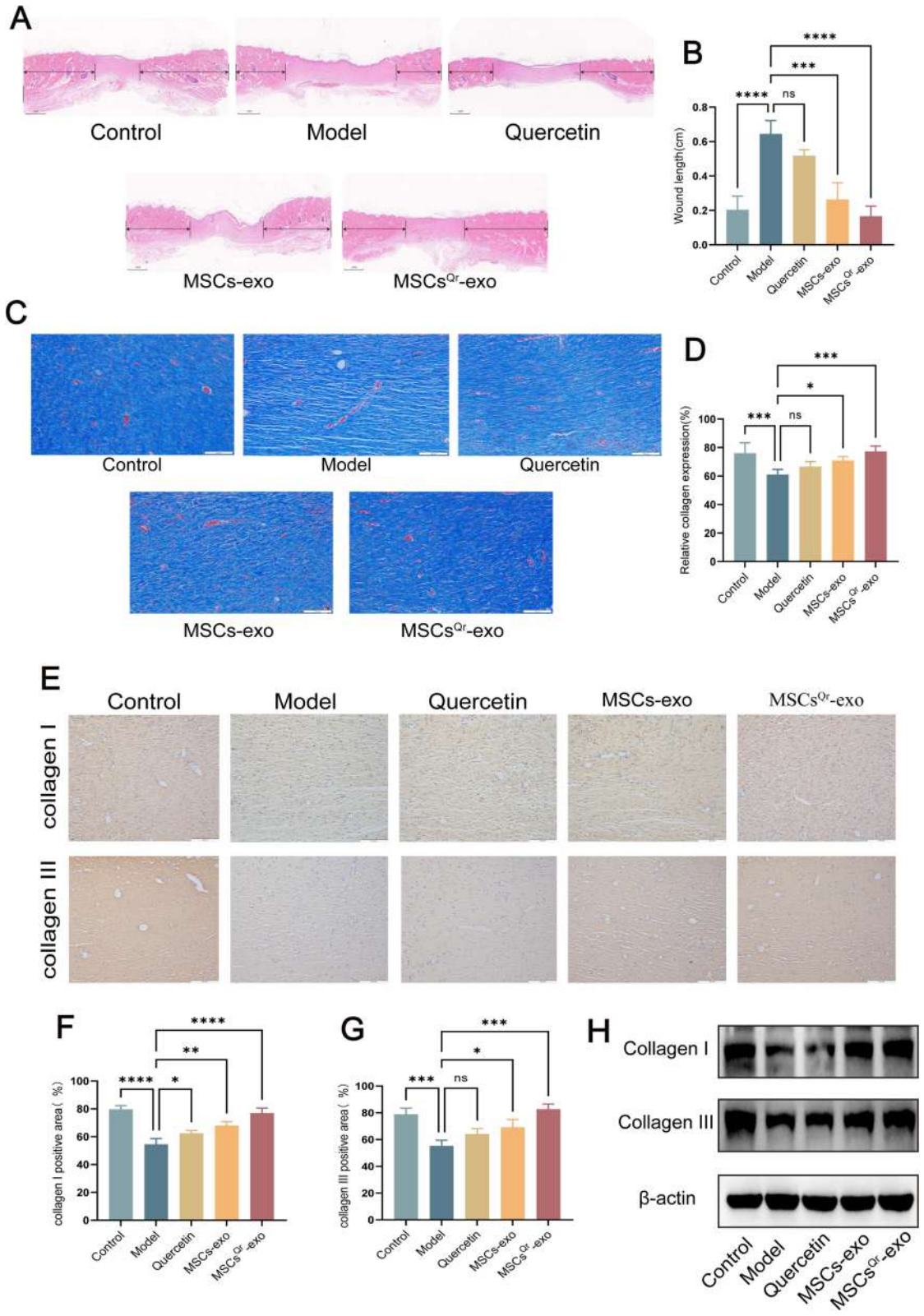

Figure 5 Histological analysis of wound tissues in DSW rats. (**A** and **B**) Representative images of H&E-stained sections of wound tissues from each group at day 21. Scale bar = 1mm. (**C** and **D**) Masson's trichrome staining performed at day 21. Scale bar = 100μm. (**E**) Immunohistochemical staining of type I collagen and type III collagen in wound tissues from each group at day 21, with representative images selected. Scale bar = 100μm. (**F** and **G**) Quantitative analysis of positive areas of type I collagen and type III collagen in each group using ImageJ software. N = 6. Comparison was made with the model group. Compared with the model group: ns: no significance, *p < 0.05, **p < 0.01, ***p < 0.001, ****p < 0.0001. (**H**) Western blot analysis was conducted to assess the expression levels of type I collagen and type III collagen. The figure employs double-headed error bars to represent the 95% confidence interval of the data.

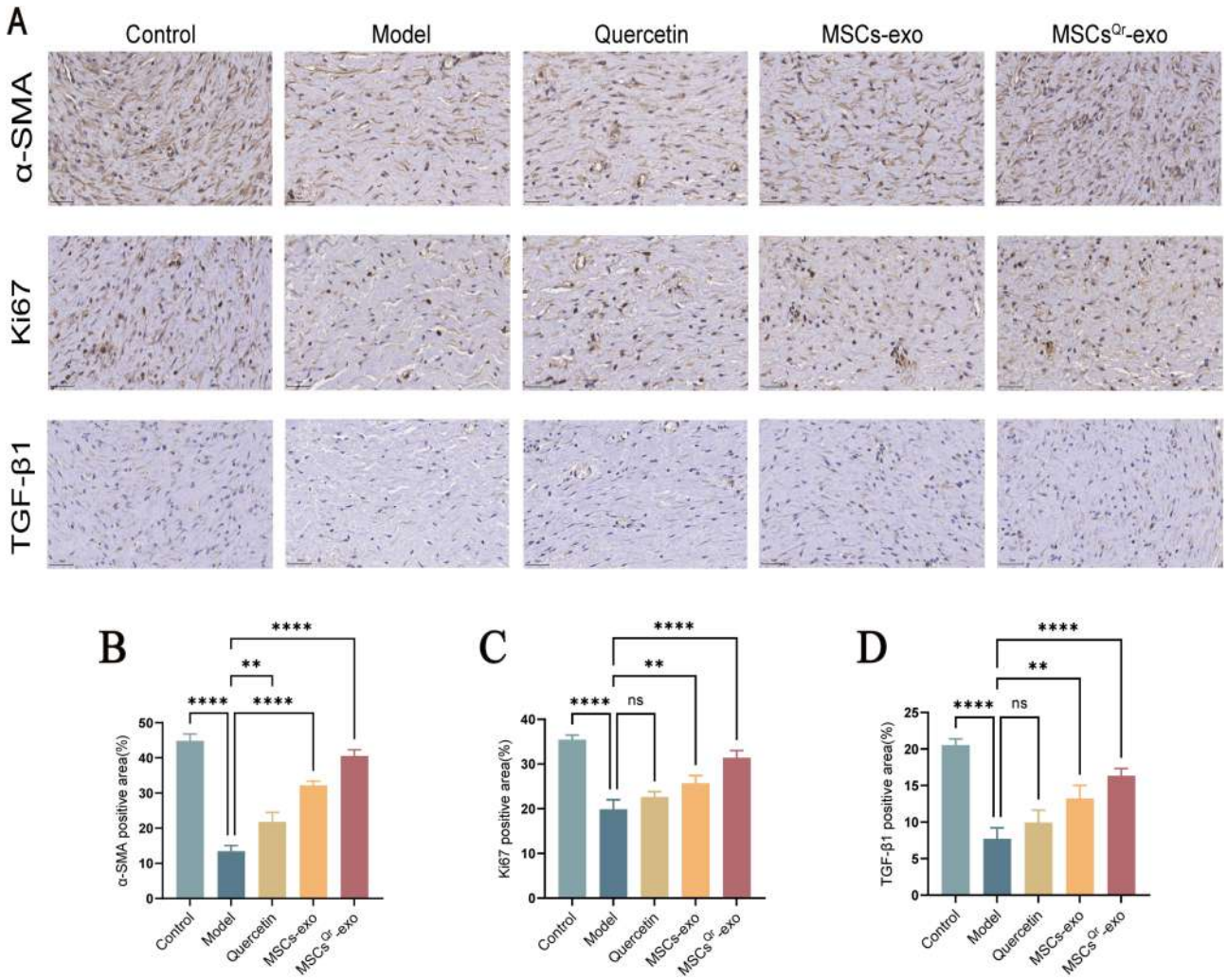

Figure 6 Immunohistochemical staining of wound tissues in various rat groups. (**A**) Immunohistochemical staining of α-SMA, Ki67, and TGF-β1 in wound tissue from rats at 21 days post-injury, with representative images selected. Scale bar = 50 μm. (**B-D**) Quantitative analysis of α-SMA, ki67, and TGF-β1 in each group using ImageJ software. N = 6. Comparison was made with the model group. Compared with the model group: ns: no significance, **p < 0.01, ****p < 0.0001. The figure employs double-headed error bars to represent the 95% confidence interval of the data.

increase in Muribculaceae_genus, whereas Clostridium_sensu_stricto_1 was significantly decreased compared to the control (Figure 7F). Furthermore, uncultured_genus and Gastranaerophilales_genus also exhibited significant differences between the two groups (Figure 7G). The results from PICRUSt2 analysis provide insights into the functional changes in the gut microbiota of DSW rats. According to predictions from the KEGG database, metabolic pathways such as Protein digestion and absorption, Lipopolysaccharide biosynthesis, Biosynthesis of siderophore group nonribosomal peptides, and Steroid hormone biosynthesis were significantly elevated in the model group, whereas pathways like Carotenoid biosynthesis, D −Arginine and D−ornithine metabolism, and Atrazine degradation were significantly decreased ($p<0.05$) (Figure 7H).

The Integration of Multi-Omics Data Reveals That MSCs^{Qr}-Exo Promotes Wound Healing in DSW Rats Through Modulation of the Gut Microbiota

In order to further explore the role of gut microbiota in the healing process of DSW, fecal samples were collected from rats across four groups: the control group, model group, MSCs-exo group, and MSCs^{Qr}-exo group. Analysis of gut microbiota composition among these groups was conducted using 16S rRNA sequencing to examine both similarities and differences. The OTU counts in the control, model, MSCs-exo, and MSCs^{Qr}-exo groups were 2855, 2460, 2325, and 2307, respectively. There were 627 OTUs shared among all four groups aPCoA demonstrated pronounced disparities in

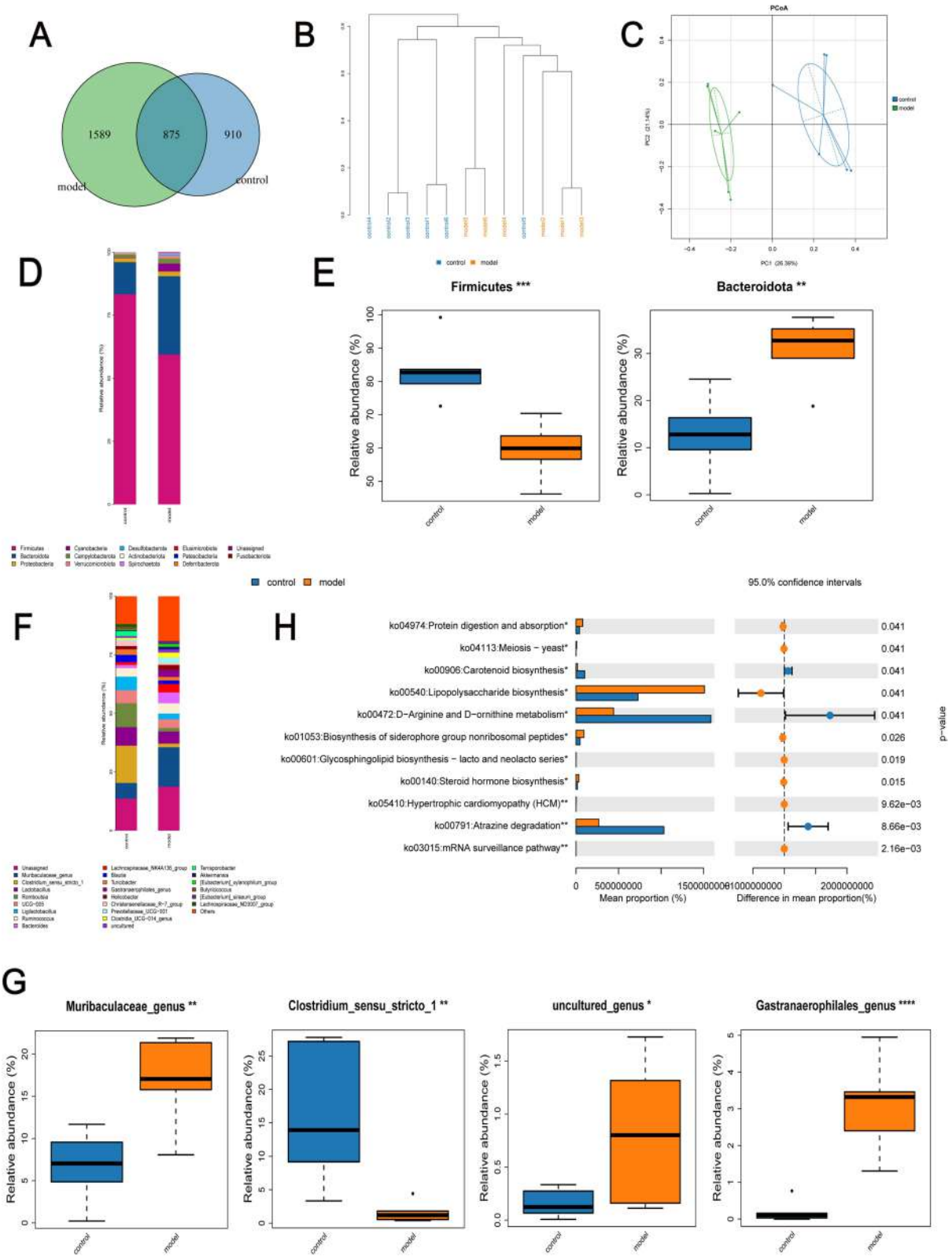

Figure 7 Changes in gut microbiota of DSW rats compared to controls. (**A**) Venn diagram used to screen unique OTUs in the model and control groups. (**B**) Dendrogram analysis of sample clustering depicting similarities and differences between model and control group samples. Samples from different groups are depicted in different colors, with branch lengths in the tree reflecting distances between samples. Closer composition indicates shorter distances between samples. (**C**) Principal coordinate analysis reflecting differences within and between groups of samples. (**D**) Analysis of relative abundance distribution of gut microbiota at the phylum level among groups. (**E**) Differences in abundance of bacterial communities at the phylum level. (**F**) Analysis of relative abundance distribution of gut microbiota at the genus level among groups. (**G**) Differences in abundance of bacterial communities at the genus level. (**H**) Prediction of differential metabolic pathways analyzed via PICRUSt2 based on 16S rRNA sequencing results. Statistical significance: *p < 0.05, **p < 0.01, ***p<0.001, ****p < 0.0001.

gut microbiota composition among the groups. Treatment with MSCs-exo and MSCs^{Qr}-exo induced alterations in gut microbiota composition in DSW rats (Figure 8B). Linear discriminant analysis effect size (LEfSe) was used to pinpoint species that might account for inter-group disparities (Figure 8C–D). The species composition histogram across multiple samples depicted the microbial community structure at the phylum and genus levels. Analysis at the phylum level revealed a notable decrease in Firmicutes compared to the control group, with both MSCs-exo and MSCs^{Qr}-exo treatments showing some degree of elevation in Firmicutes. Additionally, the abundance of Bacteroidetes was markedly higher in the model group, and treatments with MSCs-exo and MSCs^{Qr}-exo exhibited varying degrees of improvement (Figure 8E–F). At the genus level, in comparison to the control group, the model group exhibited marked reductions in Faecalibaculum, Enterorhabdus, and Clostridium_sensu_stricto_1, whereas Muribaculaceae_genus, uncultured_genus, and Gastranaerophilales_genus demonstrated significantly elevated expression levels. Following treatment with either MSCs-exo or MSCs^{Qr}-exo, the abundance of these bacteria improved to varying degrees. Notably, MSCs^{Qr}-exo exhibited superior therapeutic effects (Figure 8G–H). Using the KEGG database, we employed PICRUSt2 to predict the functional changes in the gut microbiome of DSW rats following MSCs^{Qr}-exo treatment, generating a heatmap of the 30 most abundant pathways (Figure 8I). Post MSCs^{Qr}-exo treatment, these pathways exhibited significant differences in expression (Figure 8J).

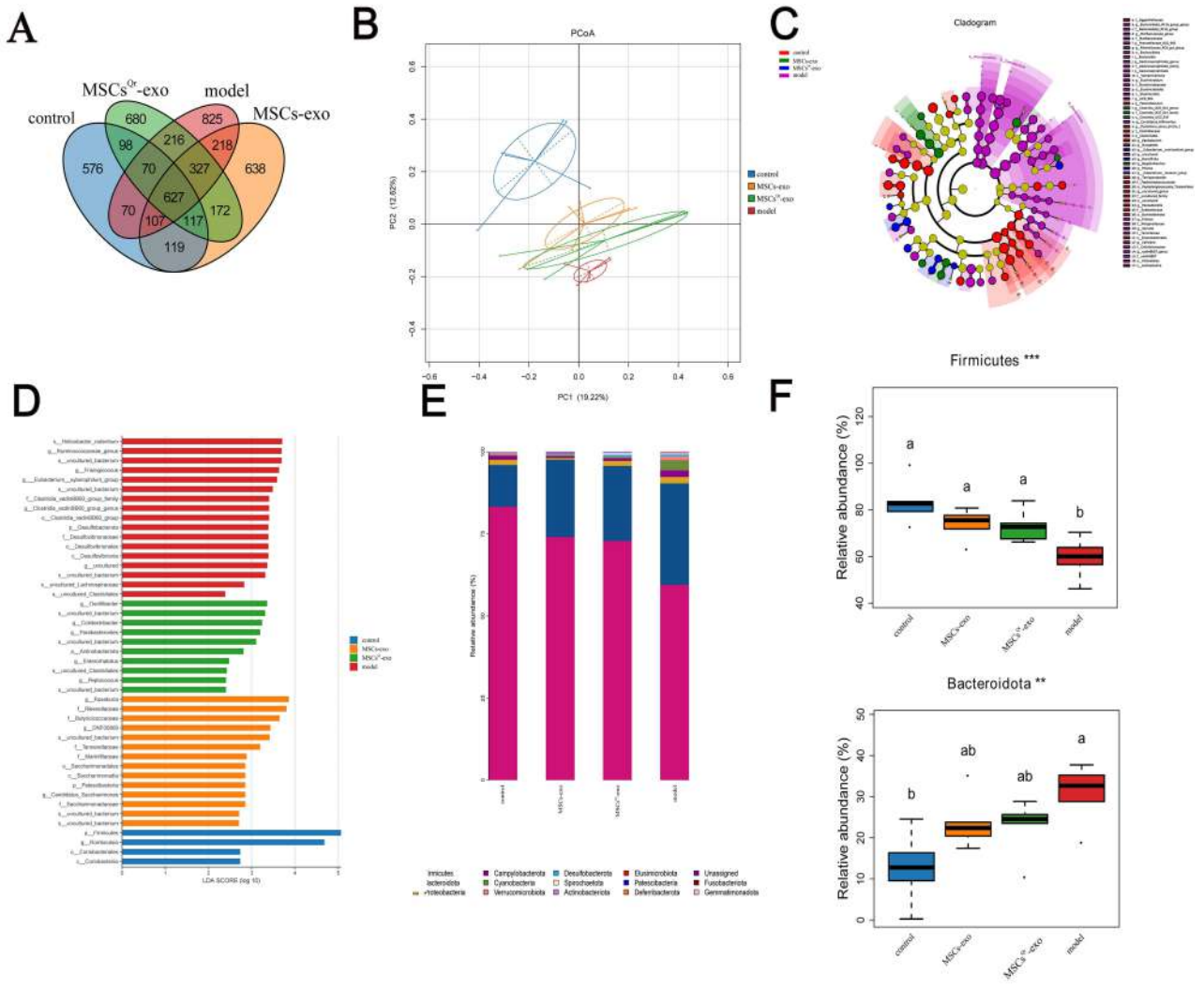

Figure 8 Continued.

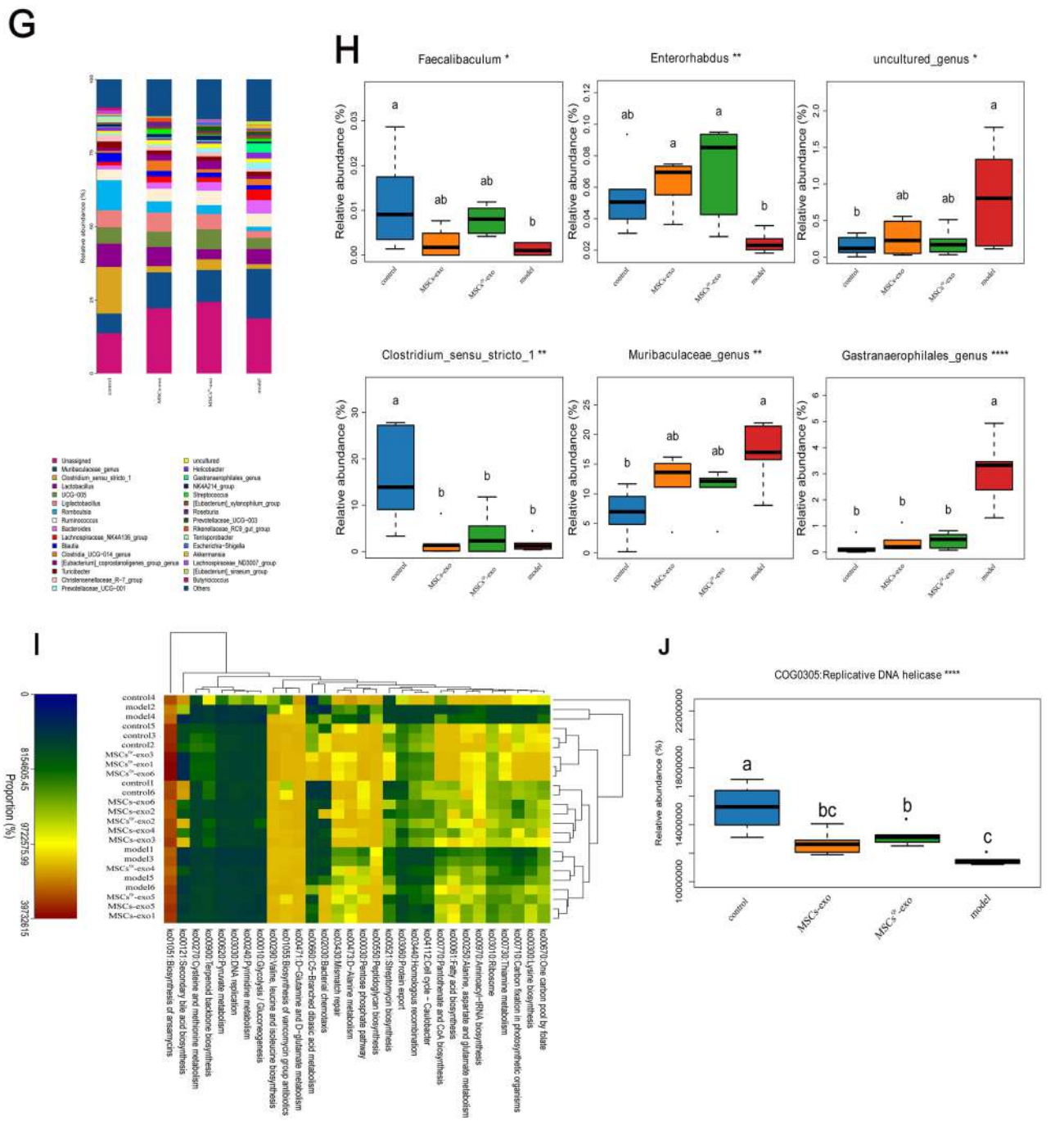

Figure 8 MSCs^{Qr}-exo promotes healing of DSW by modulating dysbiotic gut microbiota. (**A**) Venn diagram illustrating unique OTUs among the model group, control group, MSCs-exo group, and MSCs^{Qr}-exo group. (**B**) Hierarchical clustering dendrogram analyzing similarity and dissimilarity among samples from each group. Samples are color-coded to represent different groups, with branch lengths indicating distances between samples. Closer compositional similarity results in shorter distances between samples. (**C**) Linear discriminant analysis effect size (LEfSe) analyzing differences within and between groups of samples. (**D**) Relative abundance calculation of bacterial taxa analyzed via LEfSe. Each bar graph represents log10 effect size (LDA score) for specific taxonomic units. (**E**) Examination of the distribution of gut microbiota at the phylum level across different experimental groups. (**F**) Assessment of variations in the abundance of bacterial communities at the phylum level. (**G**) Analysis of the relative abundance patterns of gut microbiota at the genus level among the experimental groups. (**H**) Evaluation of differences in the abundance of bacterial communities at the genus level. (**I**) The KEGG database was used to predict functional changes in the gut microbiota of DSW rats following MSCs^{Qr}-exo treatment, identifying the top 30 pathways with significant abundance differences across the four groups. (**J**) Following MSCs^{Qr}-exo treatment, pathways exhibiting significant differential expression were observed. Statistical significance: *p < 0.05, **p < 0.01, ***p < 0.001, ****p < 0.0001. Data were analyzed using Tukey's multiple comparisons test, with "a, b" in the figure indicating significant differences between groups at a significance level of p < 0.05.

The Impact of MSCs^{Qr}-Ex Treatment on the Expression Levels of Microbial Metabolites

The alterations in microbial metabolites in rat feces were analyzed using untargeted liquid chromatography-mass spectrometry (LC-MS). Orthogonal Partial Least Squares Discriminant Analysis (OPLS-DA) was employed to detect intergroup differences, revealing significant discrepancies between the model and control groups (Figure 9A). Subsequently, the PLS-DA model was validated by randomly permuting the class variable Y and constructing corresponding PLS-DA models multiple times (n = 200), resulting in the R2 and Q2 values for the random models. The Q2 point on the far right of the resulting plot was higher than all the Q2 points marked in blue on the left, confirming the validity of the results (Figure 9B). The results of the volcano plot analysis illustrated the distribution of differential metabolites between the two groups, revealing that 151 metabolites were altered ($p<0.05$). Among these, the expression levels of 118 metabolites were upregulated, while 33 metabolites were downregulated (Figure 9C). The metabolic enrichment bubble plot reflected the altered metabolic pathways, with significant changes observed in pathways such as arachidonic acid metabolism, linoleic acid metabolism, steroid hormone biosynthesis, and neuroactive ligand-receptor interaction (Figure 9E). These pathways may contain one or more elements that play a crucial role in the pathogenesis of DSW. The relative abundance of metabolites in each sample at the same level was assessed using z-score analysis. The results indicated significant changes in metabolites such as arachidonic acid, 6-deoxy-L-galactose, myristoleic acid, 14.15-EET, formononetin, desaminotyrosine, astaxanthin, 15-deoxy-Δ12,14-PGJ, 5.6-dihydro-5-fluorouracil, N6-acetyl -L-lysine, 3-ketosphingosine, trioxilin A3, and biliverdin in the model group (Figure 9D).

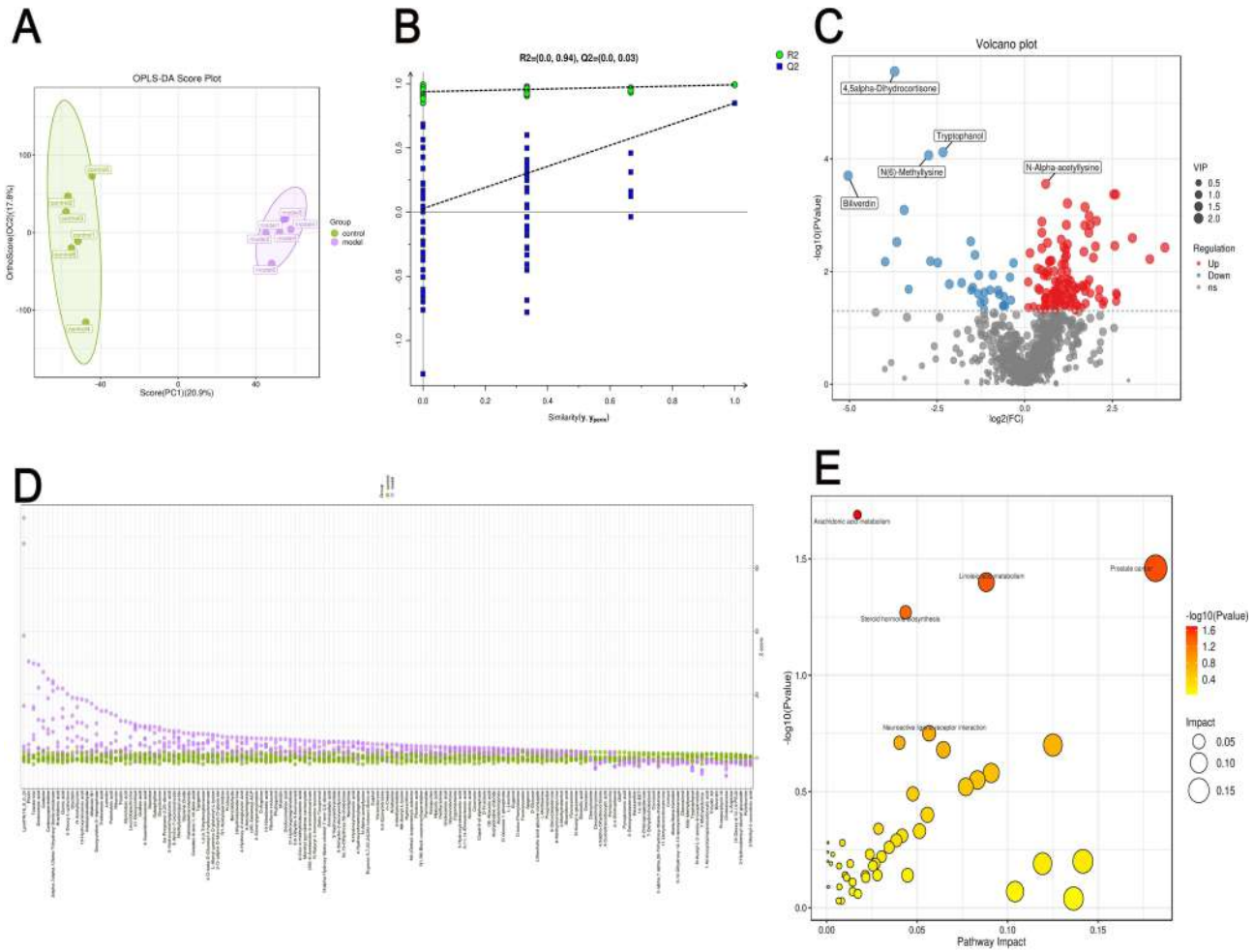

Figure 9 Continued.

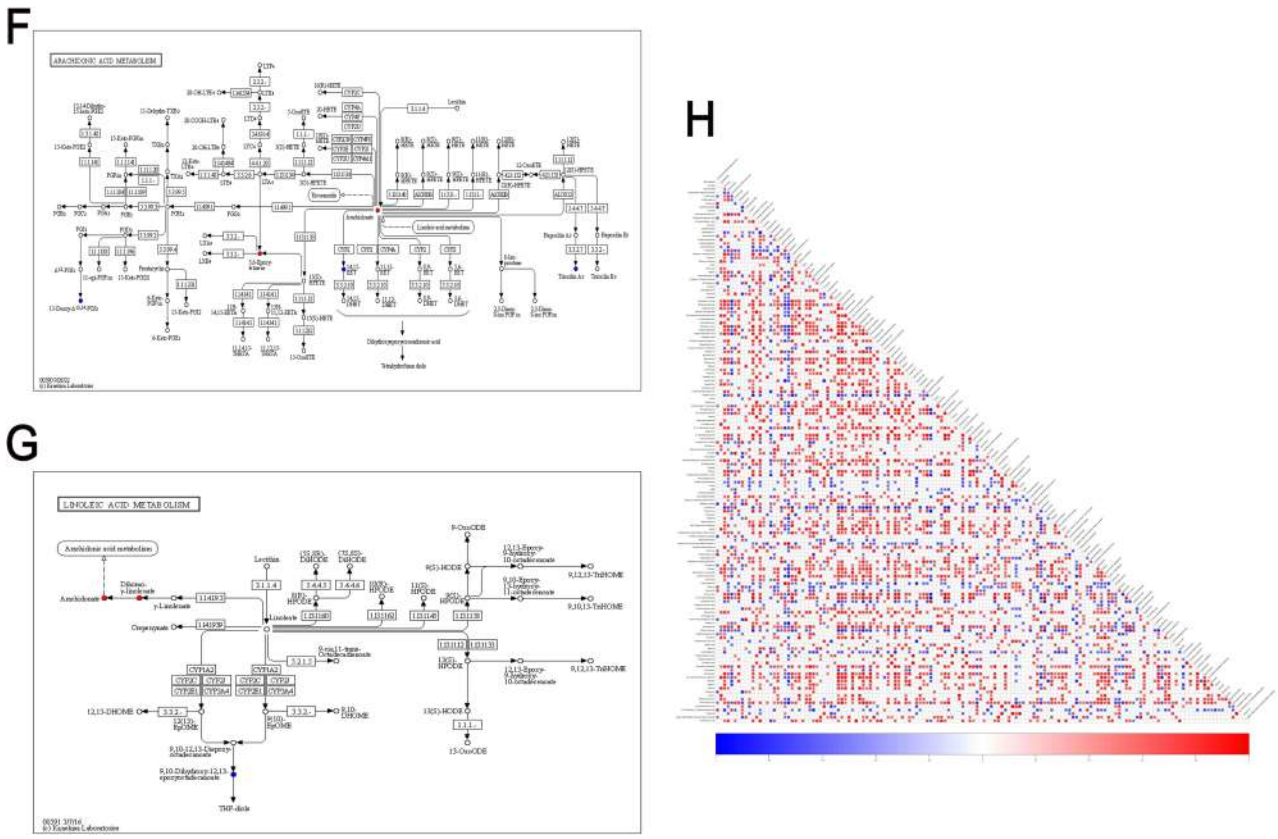

Figure 9 Metabolic changes in DSW rats compared to the control group. (**A**) Differences and reproducibility within and between groups were evaluated using OPLS-DA scores. Each point in the figure represents a sample, with different colors denoting different groups. Greater dispersion between groups and higher clustering within groups indicate more significant intergroup differences and higher intragroup reproducibility. (**B**) The statistical significance of the model was assessed through a permutation test of the PLS-DA model to prevent overfitting. All blue Q2 points shown in the figure are consistently lower from left to right than the original blue Q2 points on the far right, confirming the reliability of the results. (**C**) Differences in metabolites and their distribution between the two sample groups are illustrated by a volcano plot. Each point in the figure represents a metabolite, with red points denoting upregulated differentially expressed metabolites, blue points denoting downregulated differentially expressed metabolites, and gray points indicating metabolites that were detected but did not meet the filtering criteria. (**D**) The relative abundance of metabolites in each sample at the same level is represented by the z-score (standard score). The horizontal axis of the figure reflects the relative abundance of metabolites within the group, while the vertical axis lists the names of the metabolites. Different colors are used to represent different groups. Higher z-score values to the right indicate greater abundance of that metabolite within the group. (**E**) The metabolic pathway enrichment bubble chart derived from the pathway analysis of differential metabolites between the two groups. The x-axis represents the Impact values for various metabolic pathways, while the y-axis shows the -log10(**P**) values. A larger Impact value signifies a greater contribution of the detected metabolites to the pathway, indicating a more significant impact on the metabolic pathway. Different points on the chart represent various metabolic pathways. The color intensity of the points corresponds to the P value: darker colors indicate smaller P values, while lighter colors indicate larger P values. (**F**) Construction of the arachidonic acid metabolic pathway map. In the figure, red dots represent significantly elevated metabolites in the model group, while blue dots indicate significantly reduced metabolites in the model group. (**G**) Construction of the linoleic acid metabolism pathway. In the figure, red dots represent significantly elevated metabolites in the model group, while blue dots indicate significantly reduced metabolites in the model group. (**H**) Construction of a heatmap of differential metabolite associations, reflecting the correlations between various metabolites by calculating the correlation coefficients between each pair of metabolites. This chart can illustrate the consistency of change trends among metabolites.

Based on the aforementioned analysis, we further validated the relationship between metabolite alterations and changes in metabolic pathways. Correlation networks for arachidonic acid metabolism and linoleic acid metabolism were constructed to verify the relationship between metabolic pathways and the changes in enriched metabolites. In the arachidonic acid metabolism pathway, arachidonate was significantly upregulated in the model group, while the expression levels of 14.15-EET, 15-deoxy-Δ12,14-PGJ2, and trioxilin A3 were downregulated (Figure 9F). In the linoleic acid metabolism pathway, the expression level of arachidonate was also significantly increased, while 9.10-dihydroxy-12,13-epoxyoctadecanoate was significantly decreased (Figure 9G). In addition to the aforementioned metabolites enriched in the pathways, metabolites such as 6-deoxy-L-galactose, myristoleic acid, formononetin, desaminotyrosine, astaxanthin, 5.6-dihydro-5-fluorouracil, N6-acetyl-L-lysine, 3-ketosphingosine, and biliverdin were not enriched in the corresponding pathways. However, various studies indicate that these metabolites may play roles in the healing process of DSW. L-rhamnose (6-deoxy-L-galactose) exerts inhibitory effects on skin immune responses and activation of alveolar macrophages. Myristoleic acid induces apoptosis and necrosis in human prostate LNCaP cells.[33] Formononetin significantly inhibits proliferation, migration, and tube formation of endothelial cells.[34] Type I interferons play crucial

roles in antiviral defense and in promoting proliferation and activation of T cells and NK cells, while desaminotyrosine significantly amplifies Type I interferon signaling.[35] Astaxanthin (AST), a red carotenoid pigment, exhibits significant effects in antioxidation, anti-inflammation, and anti-apoptosis.[36] Biliverdin (BV) acts beneficially in antioxidation and targeting multiple signaling pathways, thereby benefiting ischemia/reperfusion-related diseases, inflammatory diseases, graft-versus-host disease, viral infections, etc.[37] Differential metabolite correlation heatmap results indicate significant negative correlations among 5.6-dihydro-5-fluorouracil, N6-acetyl-L-lysine, 3-ketosphingosine, and desaminotyrosine. Further research is needed to investigate their roles in the inflammatory processes of DSW injury healing (Figure 9H).

Analysis of the Interactions Between Gut Microbiota and Metabolites

Spearman correlation analysis was conducted to assess the relationship between pivotal gut microbiota and significantly altered metabolites (Figure 10). Analysis of the results indicates a positive correlation between 14.15-EET and Firmicutes, Enterorhabdus ($p<0.05$). Furthermore, KEGG pathway enrichment analysis revealed that 14.15-EET is enriched in the arachidonic acid metabolism pathway, with significantly decreased expression levels in the model group (Figure 9F). Another metabolite of interest is arachidonic acid, which shows a negative correlation with Faecalibaculum ($p<0.05$). Arachidonic acid is enriched in both the arachidonic acid metabolism pathway and the linoleic acid metabolism pathway, with significantly increased expression levels observed in DSW rats (Figure 9F–G). These

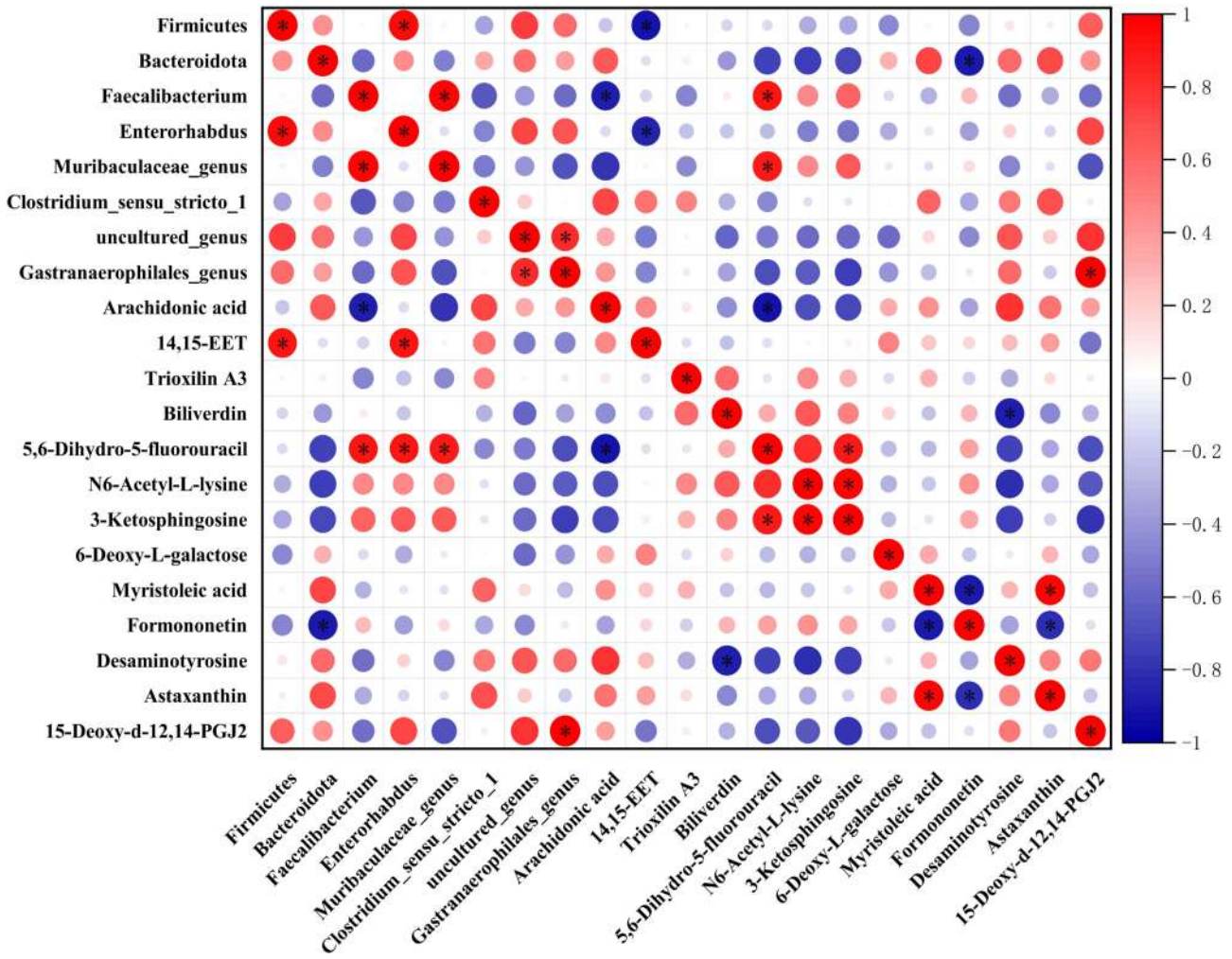

Figure 10 Correlation analysis between host microbiota and differential metabolites. The interrelationships between microbiota and differential metabolites are depicted using Spearman correlation analysis. Red points in the figure represent positive correlations, whereas blue points represent negative correlations, with * $p < 0.05$.

results reflect a certain association between changes in metabolites such as 14.15-EET and arachidonic acid with the progression of DSW, while also revealing the role of gut microbiota in the wound healing process of DSW (Figure 9H).

Discussion

In recent years, with the rapid advancement of high-throughput omics technologies, the role of gut microbiota in health and disease has become a prominent research focus. Dysbiosis of the gut microbiota is often associated with many diseases.[38] Due to advancements in high-throughput next-generation sequencing technologies and ongoing progress in microbiome research, the relationship between type 2 diabetes and its intracorporeal microbiota has garnered significant attention. Previous studies have demonstrated significant differences in the composition of gut microbiota between patients with type 2 diabetes and healthy individuals.[39] Studies have revealed that patients with type 2 diabetes experience metabolic dysregulation and chronic inflammation, accompanied by dysbiosis of the gut microbiota. The gut microbiota plays a crucial role in both metabolic regulation and immune modulation within the body. Due to dysbiosis of the gut microbiota, the intestinal barrier of diabetic patients is compromised, leading to damage in multiple organs of the body.[40] Therefore, improving the dysbiosis of the gut microbiota in patients with type 2 diabetes may be beneficial for the treatment of type 2 diabetes and its related conditions. Moreover, multiple studies have demonstrated the indispensable role of the microbiome in various skin disorders. In addition to the skin microbiota, changes in the gut microbiota have been observed in several skin diseases.[41] Therefore, the role of the gut microbiota in skin diseases represents one of the most promising research areas today. Unfortunately, the role of gut microbiota in DSW has not been extensively studied. Based on the above studies, it is reasonable to hypothesize a close relationship between DSW and gut microbiota.

MSCs are a type of multipotent cells with differentiation and immunomodulatory properties, playing a crucial role in enhancing tissue regeneration.[42] Recent studies have demonstrated that MSCs exert their effects through paracrine mechanisms. The exosomes released by MSCs through paracrine action exhibit therapeutic effects similar to MSCs themselves. As a cell-free therapy, MSCs-exo effectively avoids side effects associated with cell-based therapies such as immune rejection and ectopic tissue formation.[43] MSCs-exo possesses unique advantages in the treatment of DSW; however, its mechanism of action remains elusive. Recent studies have focused on modifying exosomes to enhance their functionality. Treatment of MSCs with Tanshinone IIA (TSA) enhances the secretion of exosomes, which upregulate miR-223-5p to inhibit CCR2 activation, thereby reducing monocyte infiltration and promoting angiogenesis, effectively enhancing the therapeutic efficacy of exosomes in myocardial ischemia/reperfusion injury.[44] Pretreatment of MSCs with atorvastatin enhances the secretion of exosomes that target the miR-139-3p/Stat1 pathway, thereby promoting macrophage polarization and playing a crucial role in cardiac repair following myocardial infarction.[45] Exosomes derived from LPS-stimulated BMSCs exhibit significant upregulation of autophagy-related protein 2 homolog B (ATG2B), thereby inhibiting macrophage STING signaling to alleviate pyogenic liver injury.[46] Quercetin's biological activities, including anti-inflammatory, antioxidant, anti-allergic, and antiviral properties, have garnered extensive scientific and medical research attention.[47–49] Additionally, quercetin exhibits preventive effects against chronic diseases such as cancer, diabetes, hypertension, and cardiovascular diseases.[50–53] Studies have indicated that quercetin exerts positive effects on diabetes and related metabolic disorders through various pathways, including modulation of the gut microbiota.[54] According to reports, quercetin promotes fibroblast proliferation and migration via the Wnt/β-catenin signaling pathway and TERT activation, while inhibiting inflammatory responses and enhancing growth factor expression, thereby playing a significant role in promoting skin wound healing.[55] Moreover, quercetin modulates macrophage polarization from the M1 to M2 phenotype, thereby suppressing inflammatory responses and promoting wound healing in diabetic ulcers.[56] However, further investigation is warranted to determine whether quercetin can enhance the therapeutic effects of MSCs-secreted exosomes on DSW healing through pretreatment, as well as its potential role in modulating DSW gut microbiota to promote healing.

To validate the role of $MSCs^{Qr}$-exo in promoting wound healing in DSW, MSCs-exo and $MSCs^{Qr}$-exo were extracted and validated through experiments including transmission electron microscopy, nanoparticle tracking analysis (NTA), and Western blot. Subsequently, the wound healing potential of $MSCs^{Qr}$-exo was assessed at both cellular and animal levels. Given the crucial role of fibroblasts in wound healing, this cellular experiment aimed to validate the effects of $MSCs^{Qr}$-exo on HSF function. Assessment of HSF proliferation and migration capabilities revealed that HG stimulation significantly attenuates these functions. Compared to MSCs-exo, $MSCs^{Qr}$-exo demonstrates a significantly enhanced ability to promote HSF proliferation and migration. At the animal level, the promoting effect of $MSCs^{Qr}$-exo was visually demonstrated. A DSW

rat model was established, and wound healing progress was observed and recorded. Throughout days 0, 7, 14, and 21, DSW rats treated with MSCs^{Qr}-exo exhibited significantly faster wound healing rates compared to other treatment groups. Histopathological examination further substantiated the therapeutic efficacy of MSCs^{Qr}-exo. Histological examination with H&E staining confirmed a significant reduction in wound length in the MSCs^{Qr}-exo treatment group. Masson's trichrome staining demonstrated that MSCs^{Qr}-exo promotes mature collagen formation, while immunohistochemistry and Western blot analyses confirmed its capacity to enhance the maturation of collagen types I and III. Additionally, α-SMA, Ki67, and TGF-β1 were identified as pivotal molecular markers closely associated with wound healing. α-SMA, a hallmark protein of myofibroblasts, plays a crucial role in wound closure and angiogenesis. The expression level of Ki67 reflects the degree of cellular proliferation activity to a certain extent. TGF-β1, a key growth factor in the TGF-β family, plays a crucial role in skin tissue wound healing. Immunohistochemical staining for α-SMA, Ki67, and TGF-β1 in different groups of rats further confirmed the significant role of MSCs^{Qr}-exo in promoting DSW healing. Based on these experimental results, it is hypothesized that MSCs^{Qr}-exo promotes wound healing in DSW rats by modulating the host gut microbiota.

Based on the hypothesis, this study compared the gut microbiota composition between model group rats and control group rats using 16S rRNA sequencing. Analysis confirmed significant differences in the gut microbiota composition between the two groups. Subsequent analysis at the phylum and genus levels revealed significant alterations in Firmicutes and Bacteroidetes in the model group compared to the control group. The model group exhibited a significant decrease in Firmicutes and a marked increase in Bacteroidetes. Previous studies have demonstrated a close relationship between dysbiosis characterized by decreased Firmicutes and increased Bacteroidetes and chronic inflammation. Additionally, Bacteroidetes are common Gram-negative bacteria characterized by an outer membrane, peptidoglycan layer, and cytoplasmic membrane. They produce byproducts such as acetic acid, propionic acid, and succinic acid during anaerobic respiration, contributing to various crucial metabolic activities in the human colon. Lipopolysaccharide (LPS), extracted from the membrane of Gram-negative bacteria, is a potent pro-inflammatory compound that markedly promotes inflammation. Succinate, produced through anaerobic respiration by Bacteroides fragilis, exacerbates inflammation activated by LPS in macrophages. The dysregulation of macrophage polarization due to hyperglycemia and oxidative stress in diabetes mellitus is intricately linked to DSW. In DSW wound sites, there is an elevated presence of classically activated macrophages (M1) and reduced alternatively activated macrophages (M2), resulting in delayed wound healing stuck in the inflammatory phase, impeding transition to the cell proliferation and migration phases.[57] This suggests that the enhanced relative expression of Bacteroides may be intimately linked to delayed wound healing in DSW rats. Interventions aimed at reducing the abundance of Bacteroides through targeted therapies and rectifying the dysregulated expression of Firmicutes and Bacteroides in the gut microbiota could potentially enhance wound healing in DSW wounds. At the genus level, Muribculaceae_genus, Clostridium_sensu_stricto_1, uncultured_genus, and Gastranaerophilales_genus show marked differences between the model and control groups. This underscores substantial changes in the gut microbiota of rats during DSW.

16S rRNA sequencing was conducted on the control, model, MSCs-exo, and MSCs^{Qr}-exo groups to elucidate the impact of MSCs^{Qr}-exo on the host gut microbiota. The findings reveal a pronounced improvement by MSCs^{Qr}-exo in alleviating gut microbiota dysbiosis in DSW rats. At the phylum level, MSCs^{Qr}-exo significantly ameliorates the dysregulation of Firmicutes and Bacteroidetes in the rat gut. At the genus level, Muribculaceae_genus, Clostridium_sensu_stricto_1, uncultured_genus, and Gastranaerophilales_genus exhibited varying degrees of improvement following MSCs^{Qr}-exo treatment. Overall, MSCs^{Qr}-exo demonstrated a more pronounced therapeutic effect compared to MSCs-exo. Faecalibaculum and Enterorhabdus also drew our attention. Numerous studies have demonstrated the close correlation between decreased Faecalibaculum expression and various inflammatory diseases. Moreover, the relative expression levels of this genus reflect the intestinal health to some extent.[58] Studies have shown that elevated oxidative stress significantly affects the O_2 levels in the intestinal lumen. As inflammation progresses, the reactive oxygen species (ROS) produced by prolonged oxidative stress exert certain effects on Faecalibacterium.[59] In diabetes, the high glucose levels in the body's microenvironment, combined with an inflammatory milieu, lead to the accumulation of advanced glycation end-products (AGEs).[60] AGEs activate relevant transcription factors, thereby inducing a state of heightened inflammation and oxidative stress in the body. Consequently, the expression levels of Faecalibacterium were markedly decreased in the model group. Treatment with both MSCs-exo and MSCs^{Qr}-exo led to varying degrees of enhancement, with MSCs^{Qr}-exo demonstrating superior therapeutic efficacy. Therefore, we can deduce that MSCs^{Qr}-exo improves Faecalibacterium expression levels in the intestines of DSW rats by reducing high levels of inflammation and oxidative stress,

thereby fostering DSW wound healing. Enterorhabdus, another genus, is intricately linked to genetic variations in human leukocyte antigen complexes, crucial in inflammatory diseases.[61] Existing studies have confirmed a negative correlation between Enterorhabdus and inflammatory bowel disease (IBD).[62] Hence, we hypothesize that the marked reduction in Enterorhabdus abundance in DSW rats contributes to the delayed healing of DSW wounds. In our study, Enterorhabdus, which was significantly reduced in the model group of rats, exhibited a marked increase in abundance following treatment with MSCs-exo and MSCs^{Qr}-exo, with MSCs^{Qr}-exo showing superior therapeutic efficacy. This may represent one of the mechanisms by which MSCs^{Qr}-exo effectively enhances wound healing in DSW.

Combining the findings from these studies, we conclude that MSCs^{Qr}-exo promotes wound healing in DSW rats by ameliorating the dysbiosis of gut microbiota. Building on this, we utilized non-targeted liquid chromatography-mass spectrometry to further investigate changes in metabolites of rat gut microbiota. The study revealed significant alterations in metabolites such as Arachidonic acid, 6-Deoxy-L-galactose, Myristoleic acid, 14.15-EET, Formononetin, Desaminotyrosine, Astaxanthin, 15-Deoxy-Δ12,14-PGJ, 5.6-dihydro-5-Fluorouracil, N6-Acetyl-L-lysine, 3-Ketosphingosine, Trioxilin A3, and Biliverdin in the model group. Arachidonic acid metabolically generates metabolites such as prostaglandins, thromboxanes, leukotrienes, lipoxins, hydroxyeicosatetraenoic acid (HETE), and epoxyeicosatrienoic acids (EETs), which play crucial roles in physiological processes like inflammation and drug metabolism, regulated by enzymes such as cyclooxygenases (COX), lipoxygenases (LOX), and cytochrome P450 (CYP450).[63] In the DSW rat model, arachidonic acid expression levels are significantly elevated, and it is enriched in both the arachidonic acid and linoleic acid metabolic pathways. Results from Spearman correlation analysis indicated a negative correlation between Faecalibacterium and arachidonic acid. From this, we can infer that decreased abundance of Faecalibacterium in the rat gut leads to elevated levels of arachidonic acid expression, which in turn delays wound healing in DSW rats. 14.15-EET has been shown to play a beneficial role in metabolic syndrome.[64] Studies indicate that 14.15-EET significantly reduces palmitic acid-induced liver cell inflammation and oxidative stress.[65] In the DSW rat model, 14.15-EET levels are markedly reduced and enriched in the arachidonic acid metabolic pathway. According to Spearman correlation analysis, Firmicutes and Enterorhabdus show a negative correlation with 14.15-EET. Thus, the decreased abundance of Firmicutes and Enterorhabdus in the gut leads to reduced levels of 14.15-EET expression, contributing to delayed wound healing in rats. Consequently, MSCs-exo and MSCs^{Qr}-exo exhibit a significant enhancement in the abundance of Firmicutes, Enterorhabdus, and Faecalibacterium in the intestines of DSW rats. Moreover, MSCs^{Qr}-exo demonstrates a stronger regulatory effect. The influence of gut microbiota on the host is mediated through metabolic products.[66] Faecalibacterium regulates the expression levels of arachidonic acid, thereby influencing its metabolic pathway. Similarly, Firmicutes and Enterorhabdus affect 14.15-EET, thereby impacting both the arachidonic acid and linoleic acid metabolic pathways.

The above conclusions may offer new insights into understanding the relationship between DSW and gut microbiota, proposing novel mechanisms by which MSCs^{Qr}-exo promotes DSW healing. However, this study has several limitations. Firstly, the use of SD rats to construct the DSW model limits its ability to reflect the complex realities of DSW patients. Secondly, this study did not perform microbiota transplantation to further validate these findings. The complex relationship between DSW and gut microbiota has been preliminarily explored, yet it has not delved deeply into the interactions between DSW, gut microbiota, and their metabolites. This suggests that future research should focus on further elucidating the impact of different gut microbiota and their metabolites on DSW, as well as exploring the interactions between gut microbiota and their metabolites. Additionally, it will be essential to further investigate the role of gut microbiota in the progression and development of DSW. This opens up new avenues and directions for future research.

Conclusion

In summary, MSCs^{Qr}-exo significantly promotes wound healing in DSW. According to 16S rRNA sequencing analysis, MSCs^{Qr}-exo regulates the disrupted gut microbiota in DSW rats, where Faecalibacterium, Firmicutes, and Enterorhabdus may play pivotal roles. Metabolomic analysis of intestinal metabolites revealed significant alterations in multiple metabolites in DSW, suggesting that interactions between the host and microbiota may be mediated through some of these metabolites. Faecalibacterium modulates arachidonic acid, thereby influencing both arachidonic acid and linoleic acid metabolic pathways, while Firmicutes and Enterorhabdus affect arachidonic acid metabolism due to their positive correlation with 14.15-EET. MSCs^{Qr}-exo exerts its pro-healing effects by improving dysregulated gut microbiota in DSW rats.

Ethical Approval

The experiment was conducted at the School of Public Health, Jilin University (SYXK (Ji) 2021-0003), under the supervision of the Institutional Animal Care and Use Committee (IACUC) of the School of Public Health, Jilin University, and in accordance with the Guidelines for Ethical Review of Laboratory Animal Welfare (GB2018-35892). The housing conditions strictly followed GB14925. Additionally, the Ethics Committee of the China-Japan Union Hospital of Jilin University approved the human ethical aspects of this study. Informed consent was obtained from all participants, and the study adhered to the principles of the Declaration of Helsinki.

Author Contributions

Shuhui Wu and Zhongsheng Zhou contributed equally to this work and share first authorship. All authors made a significant contribution to the work reported, whether that is in the conception, study design, execution, acquisition of data, analysis and interpretation, or in all these areas; took part in drafting, revising or critically reviewing the article; gave final approval of the version to be published; have agreed on the journal to which the article has been submitted; and agree to be accountable for all aspects of the work.

Funding

This work was supported by the National Natural Science Foundation of China (Grant No.8217081220), the Jilin Scientific and Technological Development Program (Grant No. 20240205001YY), the Changchun Science and Technology Development Plan Project (Grant No. 21ZGY29).

Disclosure

On behalf of all authors, the corresponding author states that there is no conflict of interest.

References

1. Guo J, Smith SM. Newer drug treatments for type 2 diabetes. *BMJ*. 2021;373:n1171. doi:10.1136/bmj.n1171
2. Mishra V, Nayak P, Sharma M, et al. Emerging treatment strategies for diabetes mellitus and associated complications: an update. *Pharmaceutics*. 2021;13(10):1568. doi:10.3390/pharmaceutics13101568
3. Armstrong DG, Tan TW, Boulton AJM, Bus SA. Diabetic Foot Ulcers: a Review. *JAMA*. 2023;330(1):62–75. doi:10.1001/jama.2023.10578
4. Li X, Jing X, Yu Z, Huang Y. Diverse antibacterial treatments beyond antibiotics for diabetic foot ulcer therapy. *Adv Healthc Mater*. 2023;12(23):e2300375. doi:10.1002/adhm.202300375
5. Manickum P, Mashamba-Thompson T, Naidoo R, Ramklass S, Madiba T. Knowledge and practice of diabetic foot care - A scoping review. *Diabetes Metab Syndr*. 2021;15(3):783–793. doi:10.1016/j.dsx.2021.03.030
6. Kushioka J, Chow SK, Toya M, et al. Bone regeneration in inflammation with aging and cell-based immunomodulatory therapy. *Inflamm Regen*. 2023;43(1):29. doi:10.1186/s41232-023-00279-1
7. Huang YZ, Gou M, Da LC, Zhang WQ, Xie HQ. Mesenchymal stem cells for chronic wound healing: current status of preclinical and clinical studies. *Tissue Eng Part B Rev*. 2020;26(6):555–570. doi:10.1089/ten.teb.2019.0351
8. Wang K, Chen Z, Jin L, et al. LPS-pretreatment adipose-derived mesenchymal stromal cells promote wound healing in diabetic rats by improving angiogenesis. *Injury*. 2022;53(12):3920–3929. doi:10.1016/j.injury.2022.09.041
9. Wei L, Xu Y, Zhang L, Yang L, Zhao RC, Zhao D. Mesenchymal stem cells promote wound healing and effects on expression of matrix metalloproteinases-8 and 9 in the wound tissue of diabetic rats. *Stem Cells Dev*. 2023;32(1–2):25–31. doi:10.1089/scd.2021.0218
10. Wu C, Liu W, Liu Y, et al. Human umbilical cord mesenchymal stem cell-derived TGFBI attenuates streptozotocin-induced type 1 diabetes mellitus by inhibiting T-cell proliferation. *Hum Cell*. 2023;36(3):997–1010. doi:10.1007/s13577-023-00868-9
11. Arya SB, Collie SP, Parent CA. The ins-and-outs of exosome biogenesis, secretion, and internalization. *Trends Cell Biol*. 2024;34(2):90–108. doi:10.1016/j.tcb.2023.06.006
12. Zhang Y, Liu Q, Zhang X, et al. Recent advances in exosome-mediated nucleic acid delivery for cancer therapy. *J Nanobiotechnology*. 2022;20(1):279. doi:10.1186/s12951-022-01472-z
13. Elahi FM, Farwell DG, Nolta JA, Anderson JD. Preclinical translation of exosomes derived from mesenchymal stem/stromal cells. *Stem Cells*. 2020;38(1):15–21. doi:10.1002/stem.3061
14. Wang S, Lei B, Zhang E, et al. Targeted therapy for inflammatory diseases with mesenchymal stem cells and their derived exosomes: from basic to clinics. *Int J Nanomed*. 2022;17:1757–1781. doi:10.2147/IJN.S355366
15. Zhou C, Zhang B, Yang Y, et al. Stem cell-derived exosomes: emerging therapeutic opportunities for wound healing. *Stem Cell Res Ther*. 2023;14(1):107. doi:10.1186/s13287-023-03345-0
16. Pastar I, Balukoff NC, Marjanovic J, Chen VY, Stone RC, Tomic-Canic M. Tomic-canic m: molecular pathophysiology of chronic wounds: current state and future directions. *Cold Spring Harb Perspect Biol*. 2023;15(4):a041243. doi:10.1101/cshperspect.a041243
17. Hong M, Li Z, Liu H, et al. Fusobacterium nucleatum aggravates rheumatoid arthritis through FadA-containing outer membrane vesicles. *Cell Host Microbe*. 2023;31(5):798–810.e797. doi:10.1016/j.chom.2023.03.018

18. Fan P, Nelson CD, Driver JD, Elzo MA, Peñagaricano F, Jeong KC. Host genetics exerts lifelong effects upon hindgut microbiota and its association with bovine growth and immunity. *Isme j*. 2021;15(8):2306–2321. doi:10.1038/s41396-021-00925-x
19. Wang Y, Zhang H, Ma G, Tian Z, Wang B. The contribution of intestinal Streptococcus to the pathogenesis of diabetic foot ulcers: an analysis based on 16S rRNA sequencing. *Int Wound J*. 2022;19(7):1658–1668. doi:10.1111/iwj.13766
20. Wang G, Lin Z, Li Y, et al. Colonizing microbiota is associated with clinical outcomes in diabetic wound healing. *Adv Drug Deliv Rev*. 2023;194:114727. doi:10.1016/j.addr.2023.114727
21. Ocansey DKW, Zhang Z, Xu X, et al. Mesenchymal stem cell-derived exosome mitigates colitis via the modulation of the gut metagenomics-metabolomics-farnesoid X receptor axis. *Biomater Sci*. 2022;10(17):4822–4836. doi:10.1039/D2BM00559J
22. Sun J, Xu G. Mesenchymal stem cell-derived exosomal miR-150-3p affects intracerebral hemorrhage by regulating TRAF6/NF-κB axis, gut microbiota and metabolism. *Stem Cell Rev Rep*. 2023;19(6):1907–1921. doi:10.1007/s12015-023-10541-1
23. Yi B, Pan J, Yang Z, et al. Mesenchymal stem cell-derived exosomes promote tissue repair injury in rats with liver trauma by regulating gut microbiota and metabolism. *Mol Cell Probes*. 2024;75:101958. doi:10.1016/j.mcp.2024.101958
24. Liu C, Lu Y, Du P, et al. Mesenchymal stem cells pretreated with proinflammatory cytokines accelerate skin wound healing by promoting macrophages migration and M2 polarization. *Regen Ther*. 2022;21:192–200. doi:10.1016/j.reth.2022.06.009
25. Jiang P, Cao P. Topical application of conditioned medium from hypoxically cultured amnion-derived mesenchymal stem cells promotes wound healing in diabetic mice. *Plast Reconstr Surg*. 2022;150(4):922e–923e. doi:10.1097/PRS.0000000000009476
26. Chu Z, Huang Q, Ma K, et al. Novel neutrophil extracellular trap-related mechanisms in diabetic wounds inspire a promising treatment strategy with hypoxia-challenged small extracellular vesicles. *Bioact Mater*. 2023;27:257–270. doi:10.1016/j.bioactmat.2023.04.007
27. Hu Y, Tao R, Chen L, et al. Exosomes derived from pioglitazone-pretreated MSCs accelerate diabetic wound healing through enhancing angiogenesis. *J Nanobiotechnology*. 2021;19(1):150. doi:10.1186/s12951-021-00894-5
28. Liu W, Yu M, Xie D, et al. Melatonin-stimulated MSC-derived exosomes improve diabetic wound healing through regulating macrophage M1 and M2 polarization by targeting the PTEN/AKT pathway. *Stem Cell Res Ther*. 2020;11(1):259. doi:10.1186/s13287-020-01756-x
29. Luo X, Bao X, Weng X, et al. The protective effect of quercetin on macrophage pyroptosis via TLR2/Myd88/NF-κB and ROS/AMPK pathway. *Life Sci*. 2022;291:120064. doi:10.1016/j.lfs.2021.120064
30. Jafarinia M, Sadat Hosseini M, Kasiri N, et al. Quercetin with the potential effect on allergic diseases. *Allergy Asthma Clin Immunol*. 2020;16 (1):36. doi:10.1186/s13223-020-00434-0
31. Kant V, Jangir BL, Sharma M, Kumar V, Joshi VG. Topical application of quercetin improves wound repair and regeneration in diabetic rats. *Immunopharmacol Immunotoxicol*. 2021;43(5):536–553. doi:10.1080/08923973.2021.1950758
32. Zhou Z, Li Y, Wu S, Liu T, Jiang J. Host-microbiota interactions in collagen-induced arthritis rats treated with human umbilical cord mesenchymal stem cell exosome and ginsenoside Rh2. *Biomed Pharmacother*. 2024;174:116515. doi:10.1016/j.biopha.2024.116515
33. Gao X, Leng C, Zeng G, Fu D, Zhang Y, Liu Y. Ozone initiated heterogeneous oxidation of unsaturated carboxylic acids by ATR-FTIR spectroscopy. *Spectrochim, Acta A Mol, Biomol, Spectrosc*. 2019;214:177–183. doi:10.1016/j.saa.2019.02.025
34. Machado Dutra J, Espitia PJP, Andrade Batista R. Formononetin: biological effects and uses - A review. *Food Chem*. 2021;359:129975. doi:10.1016/j.foodchem.2021.129975
35. Alwin A, Karst SM. The influence of microbiota-derived metabolites on viral infections. *Curr Opin Virol*. 2021;49:151–156. doi:10.1016/j.coviro.2021.05.006
36. Kohandel Z, Farkhondeh T, Aschner M, Pourbagher-Shahri AM, Samarghandian S. Anti-inflammatory action of astaxanthin and its use in the treatment of various diseases. *Biomed Pharmacother*. 2022;145:112179. doi:10.1016/j.biopha.2021.112179
37. Mancuso C. Biliverdin as a disease-modifying agent: an integrated viewpoint. *Free Radic Biol Med*. 2023;207:133–143. doi:10.1016/j.freeradbiomed.2023.07.015
38. Metwaly A, Reitmeier S, Haller D. Microbiome risk profiles as biomarkers for inflammatory and metabolic disorders. *Nat Rev Gastroenterol Hepatol*. 2022;19(6):383–397. doi:10.1038/s41575-022-00581-2
39. Mishra SP, Wang B, Jain S, et al. A mechanism by which gut microbiota elevates permeability and inflammation in obese/diabetic mice and human gut. *Gut*. 2023;72(10):1848–1865. doi:10.1136/gutjnl-2022-327365
40. Arora A, Behl T, Sehgal A, et al. Unravelling the involvement of gut microbiota in type 2 diabetes mellitus. *Life Sci*. 2021;273:119311. doi:10.1016/j.lfs.2021.119311
41. De Pessemier B, Grine L, Debaere M, Maes A, Paetzold B, Callewaert C. Gut-skin axis: current knowledge of the interrelationship between microbial dysbiosis and skin conditions. *Microorganisms*. 2021;9(2). doi:10.3390/microorganisms9020353
42. Wang T, Xue Y, Zhang W, Zheng Z, Peng X, Zhou Y. Collagen sponge scaffolds loaded with Trichostatin A pretreated BMSCs-derived exosomes regulate macrophage polarization to promote skin wound healing. *Int J Biol Macromol*. 2024;269(Pt 2):131948. doi:10.1016/j.ijbiomac.2024.131948
43. Liu C, Yang TH, Li HD, Li GZ, Liang J, Wang P. Exosomes from bone marrow mesenchymal stem cells are a potential treatment for ischemic stroke. *Neural Regen Res*. 2023;18(10):2246–2251. doi:10.4103/1673-5374.369114
44. Li S, Yang K, Cao W, et al. Tanshinone IIA enhances the therapeutic efficacy of mesenchymal stem cells derived exosomes in myocardial ischemia/reperfusion injury via up-regulating miR-223-5p. *J Control Release*. 2023;358:13–26. doi:10.1016/j.jconrel.2023.04.014
45. Ning Y, Huang P, Chen G, et al. Atorvastatin-pretreated mesenchymal stem cell-derived extracellular vesicles promote cardiac repair after myocardial infarction via shifting macrophage polarization by targeting microRNA-139-3p/Stat1 pathway. *BMC Med*. 2023;21(1):96. doi:10.1186/s12916-023-02778-x
46. Liu J, Tang M, Li Q, Li Q, Dai Y, Zhou H. ATG2B upregulated in LPS-stimulated BMSCs-derived exosomes attenuates septic liver injury by inhibiting macrophage STING signaling. *Int Immunopharmacol*. 2023;117:109931. doi:10.1016/j.intimp.2023.109931
47. Hosseini A, Razavi BM, Banach M, Hosseinzadeh H. Quercetin and metabolic syndrome: a review. *Phytother Res*. 2021;35(10):5352–5364. doi:10.1002/ptr.7144
48. Di Petrillo A, Orrù G, Fais A, Fantini MC. Quercetin and its derivates as antiviral potentials: a comprehensive review. *Phytother Res*. 2022;36 (1):266–278. doi:10.1002/ptr.7309
49. Tsai CF, Chen GW, Chen YC, et al. Regulatory effects of quercetin on M1/M2 macrophage polarization and oxidative/antioxidative balance. *Nutrients*. 2021;14(1):67. doi:10.3390/nu14010067

50. Luo X, Weng X, Bao X, et al. A novel anti-atherosclerotic mechanism of quercetin: competitive binding to KEAP1 via Arg483 to inhibit macrophage pyroptosis. *Redox Biol*. 2022;57:102511. doi:10.1016/j.redox.2022.102511
51. Wang ZX, Ma J, Li XY, et al. Quercetin induces p53-independent cancer cell death through lysosome activation by the transcription factor EB and reactive oxygen species-dependent ferroptosis. *Br J Pharmacol*. 2021;178(5):1133–1148. doi:10.1111/bph.15350
52. Abdou HM, Hamaad FA, Ali EY, Ghoneum MH. Antidiabetic efficacy of Trifolium alexandrinum extracts hesperetin and quercetin in ameliorating carbohydrate metabolism and activating IR and AMPK signaling in the pancreatic tissues of diabetic rats. *Biomed Pharmacother*. 2022;149:112838. doi:10.1016/j.biopha.2022.112838
53. Harahap U, Syahputra RA, Ahmed A, et al. Current insights and future perspectives of flavonoids: a promising antihypertensive approach. *Phytother Res*. 2024;38(6):3146–3168. doi:10.1002/ptr.8199
54. Roshanravan N, Askari SF, Fazelian S, Ayati MH, Namazi N. The roles of quercetin in diabetes mellitus and related metabolic disorders; special focus on the modulation of gut microbiota: a comprehensive review. *Crit Rev Food Sci Nutr*. 2023;63(17):2990–3003. doi:10.1080/10408398.2021.1983765
55. Mi Y, Zhong L, Lu S, et al. Quercetin promotes cutaneous wound healing in mice through Wnt/β-catenin signaling pathway. *J Ethnopharmacol*. 2022;290:115066. doi:10.1016/j.jep.2022.115066
56. Fu J, Huang J, Lin M, Xie T, You T. Quercetin promotes diabetic wound healing via switching macrophages from M1 to M2 polarization. *J Surg Res*. 2020;246:213–223. doi:10.1016/j.jss.2019.09.011
57. Wu X, He W, Mu X, et al. Macrophage polarization in diabetic wound healing. *Burns Trauma*. 2022;10:tkac051.
58. Martín R, Rios-Covian D, Huillet E, et al. Faecalibacterium: a bacterial genus with promising human health applications. *FEMS Microbiol Rev*. 2023;47(4). doi:10.1093/femsre/fuad039
59. Singhal R, Shah YM. Oxygen battle in the gut: hypoxia and hypoxia-inducible factors in metabolic and inflammatory responses in the intestine. *J Biol Chem*. 2020;295(30):10493–10505. doi:10.1074/jbc.REV120.011188
60. Li Q, Wen Y, Wang L, et al. Hyperglycemia-induced accumulation of advanced glycosylation end products in fibroblast-like synoviocytes promotes knee osteoarthritis. *Exp Mol Med*. 2021;53(11):1735–1747. doi:10.1038/s12276-021-00697-6
61. Huang CY, Zhang HP, Han WJ, et al. Disease predisposition of human leukocyte antigen class II genes influences the gut microbiota composition in patients with primary biliary cholangitis. *Front Immunol*. 2022;13:984697. doi:10.3389/fimmu.2022.984697
62. Liu B, Ye D, Yang H, et al. Two-sample Mendelian randomization analysis investigates causal associations between gut microbial genera and inflammatory bowel disease, and specificity causal associations in ulcerative colitis or Crohn's disease. *Front Immunol*. 2022;13:921546. doi:10.3389/fimmu.2022.921546
63. Frömel T, Naeem Z, Pirzeh L, Fleming I. Cytochrome P450-derived fatty acid epoxides and diols in angiogenesis and stem cell biology. *Pharmacol Ther*. 2022;234:108049. doi:10.1016/j.pharmthera.2021.108049
64. Zhang J, Yang C, Qiu H, et al. 14,15-EET involved in the development of diabetic cardiac hypertrophy mediated by PPARs. *Prostaglandins Other Lipid Mediat*. 2022;159:106620. doi:10.1016/j.prostaglandins.2022.106620
65. Yang T, Peng R, Guo Y, Shen L, Zhao S, Xu D. The role of 14,15-dihydroxyeicosatrienoic acid levels in inflammation and its relationship to lipoproteins. *Lipids Health Dis*. 2013;12(1):151. doi:10.1186/1476-511X-12-151
66. Kim CH. Complex regulatory effects of gut microbial short-chain fatty acids on immune tolerance and autoimmunity. *Cell Mol Immunol*. 2023;20(4):341–350. doi:10.1038/s41423-023-00987-1